Oriented Crystallization of Crosslinked *cis*-1,4-Polybutadiene Rubber

Kenji Saijo,[1] Yu-Ping Zhu,[1,*] Takeji Hashimoto,[1,2] Andrzej Wasiak,[1,3] Norbert Brzostowski[3]

[1]*Department of Polymer Chemistry, Graduate School of Engineering, Kyoto University, Katsura, Kyoto 615-8510, Japan*
[2]*Advanced Science Research Center, Japan Atomic Energy Agency, Tokai-Mura, Ibaraki Prefecture 319-1195, Japan*
[3]*Białystok Technical University, Białystok 15-351, Poland*

Received 11 March 2006; accepted 22 June 2006
DOI 10.1002/app.26019
Published online in Wiley InterScience (www.interscience.wiley.com).

ABSTRACT: Crosslinked *cis*-1,4-polybutadiene (PB) rubber is known to undergo crystallization during mechanical deformation. This article presents small-angle X-ray scattering (SAXS), wide-angle X-ray scattering (WAXS), and stress-relaxation studies of the structural development in crosslinked PB samples crystallized under various orientation regimes. The studies are concerned with isothermal crystallization at various temperatures (10 to −50°C) and at constant elongation ratios (1–4.5) and hence with the effects of weak-to-intermediate and high orientations on oriented crystallization versus the behavior of unoriented specimens. The results for weak-to-intermediate orientations indicate a decrease in the long spacing during crystallization, which is accompanied by an almost constant lamellar thickness as well as a significant time lag between the development of crystallinity revealed by WAXS and SAXS intensity measurements. The SAXS integral intensity shows an overshoot; that is, the intensity reaches a maximum after some crystallization time and then decreases. Stress measured during crystallization with constant elongation ratios shows decay, which depends on the isothermal crystallization temperature and elongation ratio. Although the crystallization in the weak-to-intermediate orientations is interpreted on the basis of nucleation growth, the crystallization under high orientations is best interpreted on the basis of spinodal crystallization. The most pronounced feature of structural formation during crystallization under high orientations is an almost constant long period from nearly the beginning of the crystallization, even in a timescale in which other physical quantities such as the WAXS crystallinity, SAXS integral intensity, and stress still change with time, suggesting spinodal-like crystallization, orientation-induced instability of molten network chains and their ordering, which involves spinodal-decomposition-like segregation of noncrystallizable parts (crosslinked points) and crystallizable parts (linear chains between the crosslinks) of network chains, and subsequent crystallization of crystallizable chains and pinning of the ordering process induced by crystallization. To the best of our knowledge, this work reports for the first time spinodal-like crystallization on oriented crosslinked polymer melts. © 2007 Wiley Periodicals, Inc. J Appl Polym Sci 105: 137–157, 2007

Key words: crystallization; orientation; polybutadiene; rubber; SAXS; WAXS

INTRODUCTION

The aim of this work is to investigate the development of the crystallinity and crystalline morphology during the crystallization of *cis*-1,4-polybutadiene (PB) rubber within various ranges of network-chain orientations. A range of rather small orientations is attained by the elongation of a crosslinked sample to an elongation ratio (λ) between 2 and 3.5, whereas strong orientations are achieved by the elongation of a sample to $\lambda = 4.5$. Studies have been performed by direct real-time measurements and *in situ* analysis of microscopically observable factors that are directly related to the structures of the materials. Changes occurring during the isothermal crystallization have been recorded to clarify the mechanism and dynamics of the ordering processes of the system. The following quantities have been investigated: the long period (L), the crystallite size [i.e., the lamellar thickness (D)], and the integrated scattering intensity (Q_r), as measured by time-resolved small-angle X-ray scattering (SAXS), and the degree of crystallinity (X_c) and width of the diffraction peaks, as measured by time-resolved wide-

This article is dedicated to the memory of Professor Marian Kryszewski.

Part of the work was completed while A. Wasiak was employed at the Institute of Fundamental Technological Research of the Polish Academy of Sciences (Warsaw, Poland) and while he was visiting Kyoto University as a visiting scientist (supported by the Japan Society for the Promotion of Science).

Correspondence to: T. Hashimoto (hashimoto.takeji@jaea.go.jp).
**Present address:* Research Center for Analysis and Measurement, Donghua University, Shanghai 200051, China

Contract grant sponsor: Japan–Poland Government Agreement on Scientific Cooperation; contract grant number: 77 (topic R-16).

Journal of Applied Polymer Science, Vol. 105, 137–157 (2007)

angle X-ray scattering (WAXS). Simultaneously, the relaxation of the stress has also been observed. Similar time-resolved X-ray studies on crosslinked rubbers were carried out by Koch et al.[1] and by Schultz.[2]

Crystallization is a physical process playing a major role in the structures and properties of polymeric substances and products. Our preliminary results on crosslinked rubber[3,4] have shown that the crystallization of a preoriented, amorphous specimen, when subjected to a decrease in the temperature, is strongly dependent on the λ value applied to the sample before a decrease in the crystallization temperature (T_c). The crystallinity and the occurrence of a particular morphology are also responsible for many macroscopic properties of the material.[5–8]

On the other hand, it is well known that the mechanical deformation of amorphous polymers or polymer melts leads to the orientation of polymer molecules along a certain direction (or directions) defined by the characteristics of the mechanical field applied to the sample.[9–11] The deformation of a polymeric sample (accompanied by the orientation of macromolecules) also leads to significant changes in the crystallization kinetics and in the morphology of the crystallized materials. Detailed, systematic, and direct studies of the development of the crystallinity and crystalline morphology during crystallization under various regimes of molecular orientations for a given sample are still lacking.

Most of the works from the past are confined to the study of the final structures achieved after isothermal, oriented crystallization[12–19] or to the study of the kinetics of the liquid–solid phase transition, following the changes in macroscopically observable factors such as the volume, heat content, and stress[20–24] or following microscopically observable factors such as the birefringence[25–28] indirectly related to the progress of the phase transition. In some cases, attempts to follow the kinetics by means of structural methods have been made through the investigation of samples obtained by the cessation of isothermal crystallization through the quenching of the samples before the process has been completed.[29] Any eventual contribution of structures arising because of and during quenching has been neglected. In particular, simultaneous studies of several diffraction techniques coupled with macroscopic techniques are lacking. Consequently, our knowledge about structural development in preoriented systems appears incomplete, limited only to some aspects not combined into a more general picture. This work aims to provide a general, integrated picture of the crystallization and evolution of the morphology of crosslinked rubbers at fixed λ values and at various T_c values.

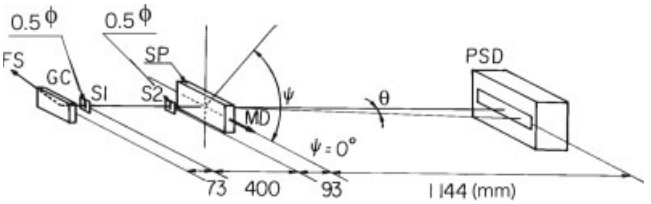

Figure 1 Optics of the SAXS instrument [FS = point-focus X-ray beam; GC = graphite monochromator crystal; PSD = position-sensitive detector; SP = sample; ψ = azimuthal angle of the SAXS intensity distribution, which can be varied by the rotation of the elongation direction (MD) of the sample].

EXPERIMENTAL

Materials

PB was chosen as a test specimen. The rubber network was first stretched uniaxially to a given λ value (λ = 1.0–4.5) and then crystallized isothermally at T_c (T_c = −50 to 10°C) while kept at a constant value of λ. Samples were kindly supplied by Assoreni (San Donato Milanese, Italy) through Ziabicki. PB was polymerized with a uranium catalyst that had 99% *cis*-1,4-linkages and a number-average molecular weight of 1.2×10^5 in the uncrosslinked state and corresponded to the sample coded Uranium C in the article by Chirico et al.[30] The polymer was crosslinked with Sulfasan R (4.4′-dithiomorpholine) with a crosslink density of 1×10^{-4} mol/cc and a number-average molecular weight between crosslinks (M_c) of 9000. The rubber network at rest (λ = 1) had a nominal melting temperature (T_m) of ≈−3°C. The M_c value of 9000 corresponded to a number-average degree of polymerization of 167, so the extended chain between the crosslinks could have 72 nm for *cis*-1,4-linkages on the basis of the crystal structure of PB.[31] From this viewpoint, the elongated network chains may still be incorporated into lamellar crystals of D = 5–9 nm (as will be elucidated later in Fig. 14) via intrachain and/or interchain crystallization into lamellae.

Time-resolved X-ray scattering measurements

Because the detailed features of the apparatus have been presented elsewhere,[32] only a brief description of the experimental techniques is presented here.

Apparatus for SAXS

The optics of the SAXS apparatus are presented in Figure 1. An X-ray beam originating from a point-focus source (effective area = 1 mm^2) in a 12-kW rotating-anode X-ray generator was monochromatized by a graphite crystal and collimated into a parallel beam by a pair of pinholes (S1 and S2; each had a diameter

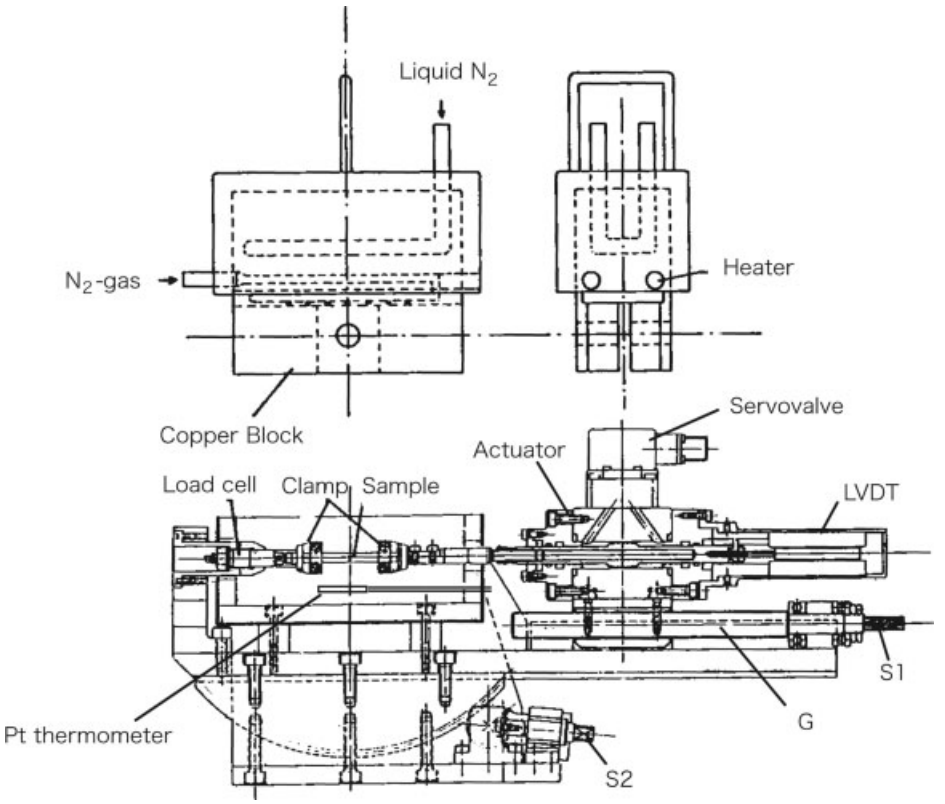

Figure 2 Sample deformation apparatus used for SAXS experiments. The apparatus comprises a hydraulic deformation device with sample clamps, gear S1 for static stretching, gear S2 for the rotation of the elongation axis in the plane normal to the primary beam, and copper blocks to control the sample temperature.

of 0.5 mm). The scattered beam from the sample was detected as a function of the scattering angle (θ) by means of a linear position-sensitive detector. The dependence of the azimuthal angle (ψ) of the scattered X-rays was measured by the rotation of the elongation direction around the axis of the incident beam in the plane normal to the incident beam.[33,34] The beam path was evacuated to avoid air scattering.

Deformation was conducted by means of a hydraulic deformation device presented in Figure 2. Several available deformation modes, such as deformation under a constant stress or constant strain, a transient mode with high-speed elongation, and an oscillatory mode with sinusoidal elongation and shear deformation, were available under computer control. The deformation axis could be rotated around the axis of the incident beam from the horizontal position to the vertical position in the plane perpendicular to the propagation direction of the incident X-ray beam to ensure the measurements of the SAXS intensity as a function of ψ by the rotation of gear S2. The stress applied to the sample was detected by a stress transducer (load cell), and the displacement of the actuator (i.e., the sample deformation) driven by the hydraulic pump was measured by a linear variable differential transformer (LVDT). The static strain could be imposed on the sample by the horizontal movement of the actuator along the guide (G) by the rotation of gear S1. Changes in the stress were monitored during the time of the measurements.

The temperature enclosure consisted of two copper blocks. One (lower) was mounted on the deformation device, and the second (upper) was removable from and fixed onto the lower block. The temperature of the specimen was maintained with an accuracy of $\pm$ 1°C through the control of the temperature of the upper block. The block consisted of two heating elements and channels for liquid nitrogen flow inside the block. When the block was fixed inside the hollow in the lower block, the specimen was contained in a narrow gap that formed between the temperature-controlled blocks. The incident X-ray beam propagated normal to the elongation axis of the sample. A detailed description of the apparatus has been given elsewhere.[32,33]

Typical examples of the time evolution of SAXS profiles along $\psi = 0^\circ$ during crystallization induced by a rapid temperature drop of an elongated crosslinked rubber sample are shown in Figure 3. q is the magnitude of scattering vector **q**:

$$q = \frac{4\pi \sin(\vartheta/2)}{\lambda} \tag{1}$$

where λ is the wavelength of the X-ray (0.1542 nm). The details of the results presented in Figure 3 are discussed later.

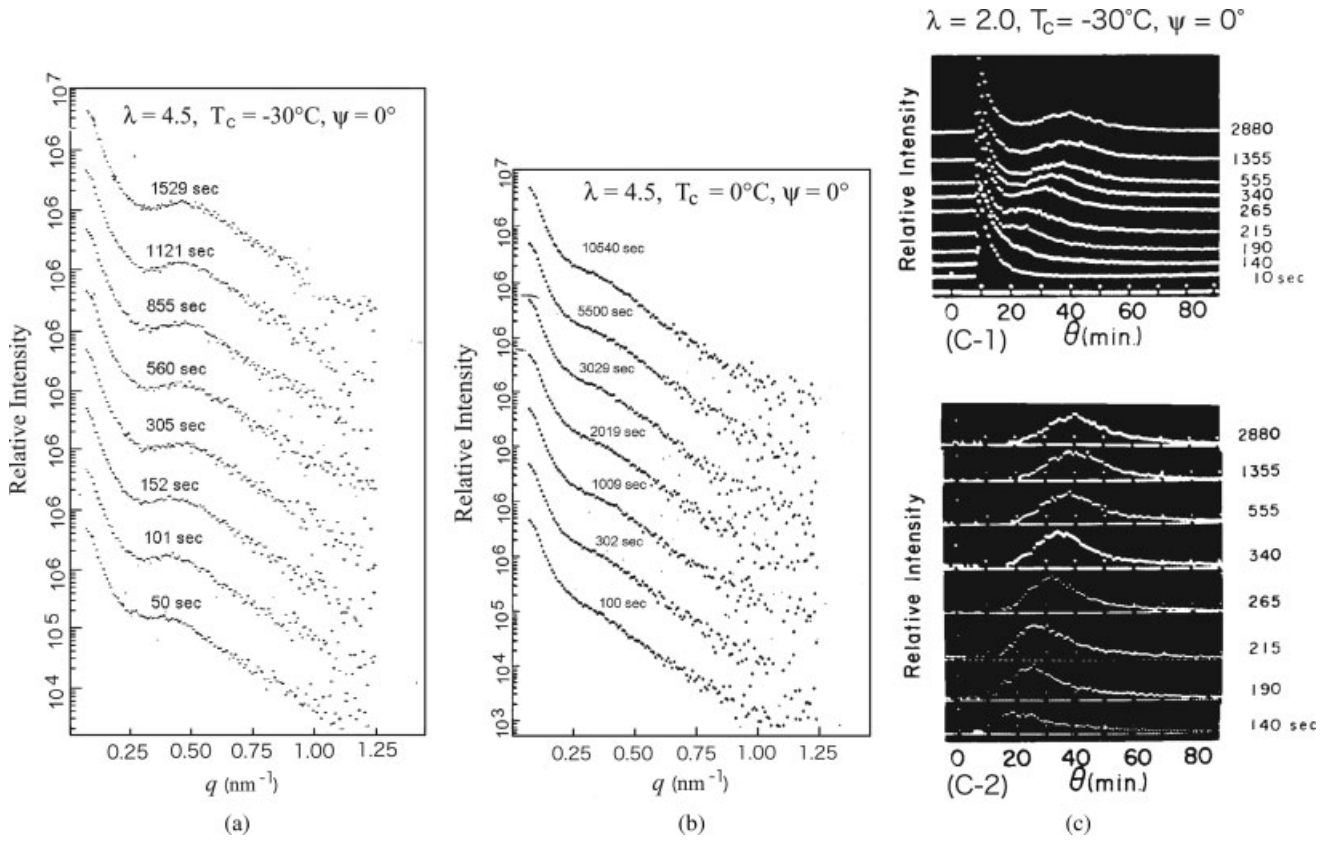

Figure 3 Time-resolved SAXS profiles measured along the elongation axis ($\psi = 0°$) during crystallization at λ and T_c: (a) $\lambda = 4.5$ and $T_c = -30°C$, (b) $\lambda = 4.5$ and $T_c = 0°C$, and (c) $\lambda = 2.0$ and $T_c = -30°C$. Each scattering profile has been shifted vertically to avoid overlapping. Part c-1 shows the SAXS intensity versus θ on a linear scale, and part c-2 shows the intensity profile obtained after the subtraction of the background scattering (the intensity profile for the same sample at melting). In part c-1, the drop in the SAXS intensity at $\theta < 10$ min is due to the beam stop placed in front of the position-sensitive detector.

Apparatus for WAXS

WAXS measurements were carried out with the same X-ray optics used for the SAXS measurements, but a different oven and sample holder were used, and the sample-to-detector distance was appropriately reduced. The design of the oven is shown in Figure 4. The oven was built from a thick block of copper, in the top of which holes were made in which a sample holder, electric heaters, and a Pt resistance thermometer could be inserted. The block itself was shielded by the insulator. The thermometer was connected to a temperature controller. Some channels were also made inside the block that could be used for cooling by means of a stream of liquid nitrogen or other cooling medium. In one side of the block, a hole was made to transmit X-ray beams, as shown in the figure. This hole had a cylindrical shape and an approximately 5-mm diameter on the side of the entrance of the primary X-ray beam and a conical shape on the other side to form an undisturbed path for scattered beams. Both sides of the hole were covered by thin aluminum foil to prevent heat loss. The sample, deformed in a separate stretching device, was placed in the sample holder and fixed by screws to keep a constant length during the crystallization experiment. The sample holder, containing the mounted sample, was inserted into the oven.

Typical time-resolved WAXS curves obtained for two representative crystallization conditions are demonstrated in Figure 5(a,b), where 2θ is the Bragg angle. The figure demonstrates changes in the scattering profile with time due to crystallization as well as the deconvolution of the net diffraction curve into the individual profiles corresponding to the amorphous region, crystallographic planes, and background scattering. The details are described later.

Data evaluation

SAXS

First, SAXS from the melt of stretched network chains arises from chain-folded-type, lamellar crystals, or bundle-type, extended-chain crystals that have developed by oriented crystallization. Thermal density fluctuations from the molten matrix of the crosslinked net-

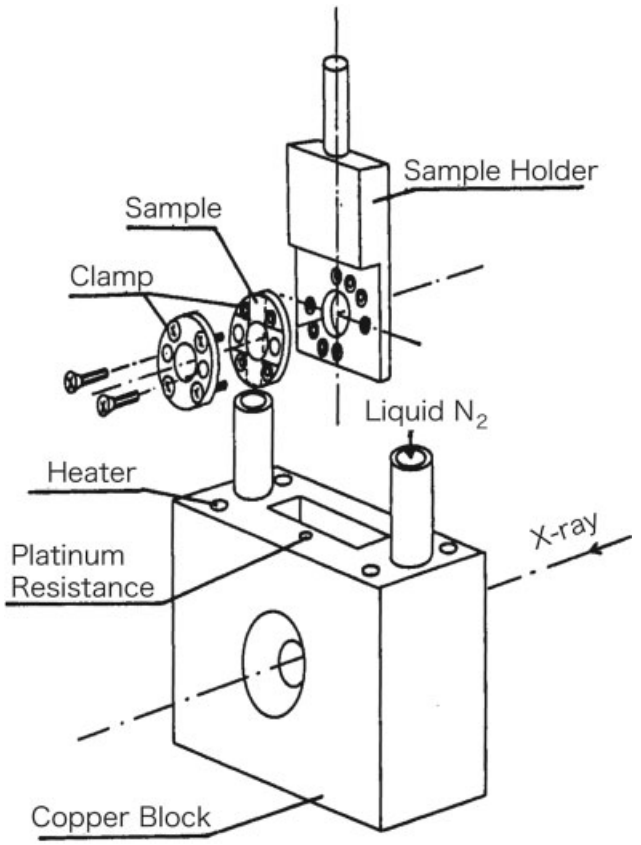

Figure 4 Temperature enclosure and sample holder for WAXS measurements. The temperature enclosure is made of a copper block with holes for incident and scattered X-rays as well as a sample holder, tubes for cooling the liquid, and heaters. Separately, a sample holder is shown with a sample and mounting clamp in the upper part of the figure.

work chains hardly contribute to the SAXS profile in the q range covered in this work.

SAXS profiles measured during oriented crystallization were first corrected for the background scattering which were measured with the same samples used for the oriented crystallization but in a molten state. The correction was done by the subtraction of the background scattering from the measured SAXS profiles. From the corrected SAXS intensity distribution [$I(q)$] along the elongation direction ($\psi = 0^\circ$), a one-dimensional correlation function [$\gamma_1(r)$] for oriented stacks of lamellae was calculated:

$$\gamma_1(r) = \int_0^\infty \mathrm{d}qI(q)q^2\cos(qr) \Big/ \int_0^\infty \mathrm{d}qI(q)q^2 \qquad (2)$$

The typical shape of the correlation function thus evaluated is demonstrated in Figure 6 for a sample at a given time during the isothermal crystallization. The figure shows how D and L can be determined.[35]

At the early stage of crystallization, in which only a monotonous decrease in the SAXS intensity was observed, the scattered intensity distribution at small angles was analyzed also by means of Guinier and Fournet's theory,[36] according to which the SAXS intensity scattered by a dilute system of particles (lamellar crystals in this work) having an average radius of gyration (R_g) can be expressed as follows:

$$I(q) \propto \exp\left(-\frac{R_g^2}{3}q^2\right) \qquad (3a)$$

From the Guinier plot of $I(q)$ at $\psi = 0^\circ$, as illustrated in Figure 7, R_g for structural entities appearing in the system was determined. The observed deviations of the data points from the straight lines at the small q limit in the figure are thought to arise from constructive interference of the scattering from the structural entities because of their finite concentrations in the systems. R_g is a weighted average of the size of a structural entity and provides information about the size of the chain-folded lamellae or bundle-type, extended-chain crystals at early stages of crystallization when periodic structures are not yet formed. We can reasonably assume that lamellar normals or the axes of the bundles are parallel to the draw direction. Under the experimental conditions in which **q** is parallel to the draw direction, $I(q)$ is given by

$$I(q) \propto \left\{\sin^2\left(\frac{qD}{2}\right)\right\} \Big/ \left(\frac{qD}{2}\right)^2 \cong \exp\left(-\frac{D^2}{12}q^2\right) \qquad (3b)$$

where $qD \ll 1$.

From eqs. (3a) and (3b), we can obtain

$$D = 2R_g \qquad (4)$$

This formula can be used for evaluating D from the Guinier plot.

The other characteristic that can be evaluated from SAXS curves is Q_r, which is proportional to the mean-square of the electron density fluctuations in a sample:[36]

$$Q_r = \int q^2 I(q)\mathrm{d}q \propto \phi_c(1-\phi_c)(\rho_c - \rho_a)^2 \qquad (5)$$

For two-phase systems, Q_r is proportional to the electron density difference between scattering entities (ρ_c) and the matrix (ρ_a) in which they are embedded [the second line of eq. (5)]. It also depends on the volume fraction of one of those entities (ϕ_c).

WAXS

WAXS provides information about the lattice structure of the crystal as well as the content of the crystalline part of the materials (X_c). The kinetics of crystallization can be studied by an analysis of the time changes in WAXS. To determine the crystallinity, the intensity profile is separated into two contributions: a broad halo arising from the amorphous component (I_{am}) and a set of narrow diffraction lines corresponding to diffractions from individual crystallographic

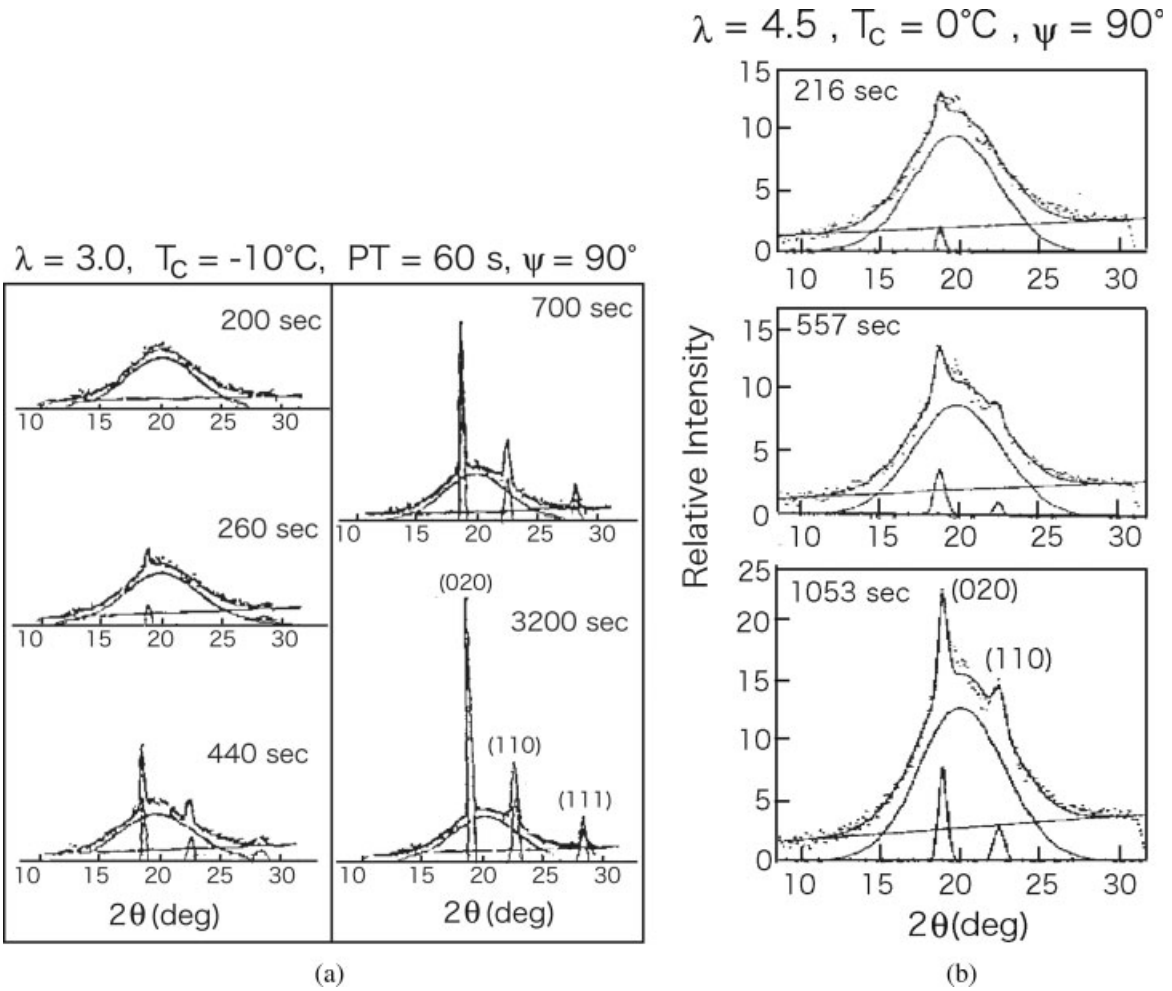

Figure 5 Development of equatorial WAXS profiles ($\psi = 90^\circ$) at various time during the crystallization of specimens (a) elongated to $\lambda = 3.0$ and crystallized at $T_c = -10^\circ$C and (b) elongated to $\lambda = 4.5$ and crystallized at $T_c = 0^\circ$C. The decomposition of the scattering curves into components corresponding to an amorphous halo, individual diffraction lines from crystals, and background scattering is also shown by the solid lines. The measured profile is shown by dots, whereas the sum of the decomposed scattering components is shown by the solid lines. PT is the counting time required to obtain each diffraction profile.

planes in the crystals (I_{cr}). X_c in an oriented system is determined as the ratio of azimuthally integrated WAXS patterns for all diffraction profiles from crystals ($\langle\langle I_{cr}(q)\rangle\rangle$) to those for all diffraction profiles including an amorphous halo ($\langle\langle I_{\mathrm{tot}}(q)\rangle\rangle$):

$$X_c = \frac{\int_{q_{\min}}^{q_{\max}} q^2 \langle I_{cr}(q)\rangle \mathrm{d}q}{\int_{q_{\min}}^{q_{\max}} q^2 \langle I_{\mathrm{tot}}(q)\rangle \mathrm{d}q} \tag{6}$$

The angular brackets denote the integration of the diffraction intensity with respect to ψ:

$$\langle I\rangle = \int_0^{\pi} I(\psi) \sin\psi \, \mathrm{d}\psi \tag{7}$$

$q_{\min}$ and $q_{\max}$ are the lower and upper bounds of q, respectively. The total intensity (I_{tot}) is given by $I_{\mathrm{tot}} = I_{cr} + I_{am}$. In eqs. (6) and (7), we assume uniaxial symmetry for the crystal and amorphous chain orientation and WAXS intensity distribution along the elongation axis. The assumption is quite legitimate in our experimental systems.

The relative crystallinity (X_{rel}) can be estimated from the WAXS intensity integrated with q only at one ψ value, such as the equatorial direction ($\psi = 90^\circ$) of the X-ray pattern. This quantity is expressed as follows:

$$X_{\mathrm{rel}} = \frac{\int_{q_{\min}}^{q_{\max}} q^2 I_{cr}(q;\psi) \mathrm{d}q}{\int_{q_{\min}}^{q_{\max}} q^2 I_{\mathrm{tot}}(q;\psi) \mathrm{d}q} \tag{8}$$

X_{rel} can be estimated from quick measurements of the intensity profile carried out by means of a one-dimensional position-sensitive proportional counter. In most cases in which the orientation of growing crystals does not vary much during the course of oriented crystallization at fixed values of λ and T_c, X_{rel} is a correct measure of the relative change in X_c with time during the crystallization process. When the

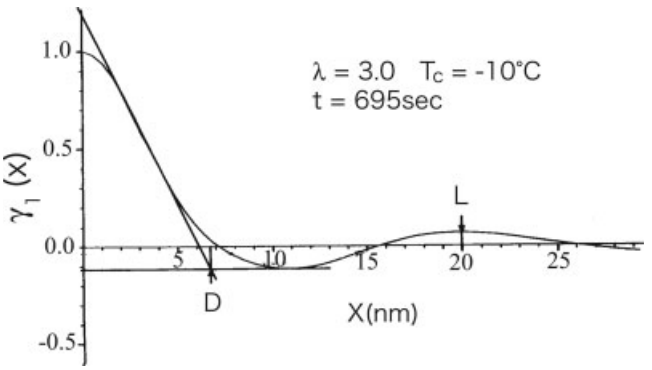

Figure 6 One-dimensional correlation function [$\gamma_1(x)$] evaluated from meridional SAXS intensity distributions ($\psi = 0^\circ$). x is the distance along the elongation direction. D is determined from the intersection of the two tangents of $\gamma_1(x)$ at small values of x and at x values at which $\gamma_1(x)$ reaches the first constant value. L is determined from the value of x at which $\gamma_1(x)$ reaches a maximum value, if there is a maximum.

WAXS intensity changed very slowly with time or after the WAXS intensity reached a steady value with time, we measured both X_c and X_{rel} and estimated the correction factor (X_c/X_{rel}), which was used to convert $X_{rel}(t)$ to $X_c(t)$, where t is the time spent for crystallization.

RESULTS AND DISCUSSION

Weak-to-intermediate orientations

We classified the oriented crystallization at fixed λ values ranging from 2.0 to 3.5 and at $T_c = -30$ to -10°C as crystallization under weak-to-intermediate orientations. To highlight the effects of λ on the crystallization, we will present our results on $L(t)$, $Q_r(t)$, and the half-time of crystallization ($t_{1/2}$) as measured by SAXS and WAXS separately and discuss how each structural parameter depends on the crystallization conditions specified by given sets of λ and T_c. $t_{1/2}$ will be defined later.

The time evolution of SAXS at $\lambda = 2.0$ and $T_c = -30^\circ$C is shown in Figure 3(c) as a typical example of crystallization under weak-to-intermediate orientations. The SAXS profiles represent those at $\psi = 0$, that is, the meridional SAXS profiles parallel to the elongation direction collected at the given times during crystallization. Two features characterizing the observed changes in the two-point SAXS patterns can be distinguished; the first concerns variations of the integral intensity, and the second concerns a shift of the position of the maximum intensity toward higher θ values. An increase in the value of q (defined by q_m) at the scattering maximum indicates that $L = 2\pi/q_m$ decreases with the crystallization time.

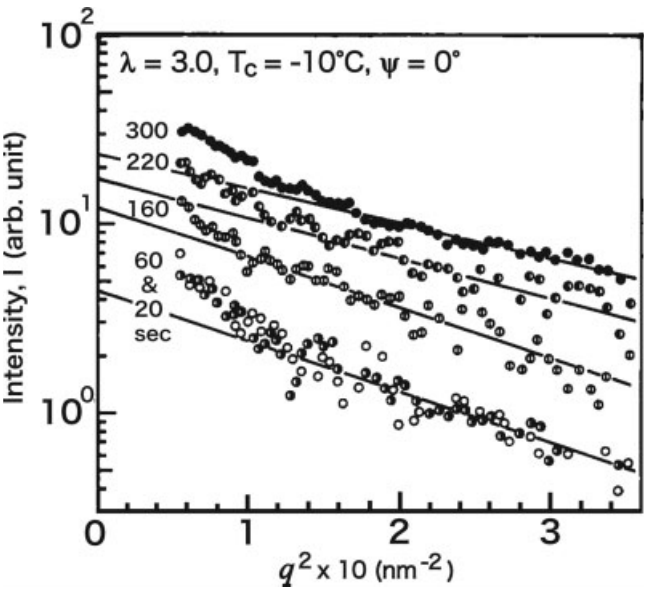

Figure 7 Guinier plots of the meridional SAXS intensity distribution ($\psi = 0^\circ$) for early stages of crystallization at $\lambda = 3.0$ and $T_c = -10^\circ$C.

The time evolution of L during the crystallization at $T_c = -10^\circ$ to -30°C for the samples elongated to λ in the range of $2.0 \leq \lambda \leq 3.5$ is summarized in Figure 8. A decrease in L occurs faster at the beginning of the process and more slowly later, and it reaches saturation in the long time limit. The changes in L with time t at a given T_c appear earlier for the samples elongated

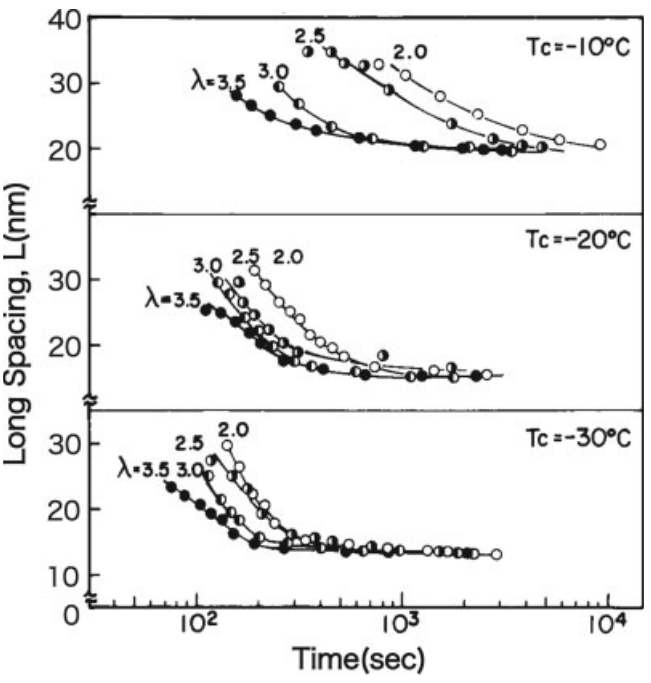

Figure 8 Time dependence of L for a few values of λ and T_c.

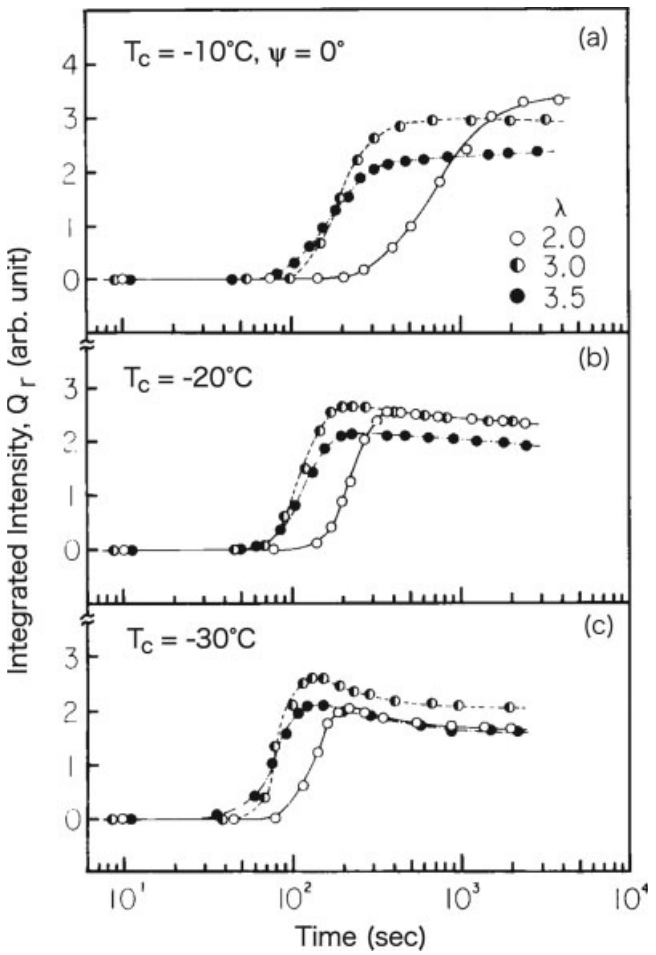

Figure 9 Time evolution of Q_r for samples elongated to various λ values and crystallized at various T_c values.

to a larger extent. Reducing T_c at a given λ value also causes an earlier appearance of the change in L. The level of saturation appears to be a function of T_c. The lower T_c is, the smaller L is at a given time and at the long time limit as well. The decrease in L was interpreted on the basis of ''car parking problems in a fixed parking area'' as the simplest possible model.[33]

As mentioned earlier, Q_r (SAXS) also varies with the crystallization time, as shown in Figure 9. The results are presented for a few λ values as well as a few T_c values. In all cases, after some initial period of a constant and low value of Q_r, an increase can be observed to the point at which a leveling off of the intensity change with time occurs. At all temperatures, time changes in Q_r for the samples elongated to $\lambda = 3.0$ and $\lambda = 3.5$ occur earlier than those for the sample elongated to $\lambda = 2.0$; The effect of increasing λ on Q_r versus t shows the shift of the sigmoidal curve toward a shorter time (a decrease in the induction period), the shape of the sigmoidal variation remaining essentially unaltered. For a given value of λ, the lower T_c is, the earlier the changes occur in Q_r. In the samples elongated to a higher degree, the T_c dependence of Q_r versus t is less evident, as can be more clearly discerned in Figure 10, in which $t_{1/2}$ as defined in the inset is shown as a function of T_c.

Q_r in the final stage of crystallization also shows some differences, depending on T_c. In the samples crystallized at -10°C, the intensity reaches saturation and remains constant, whereas in the samples crystallized at lower temperatures, Q_r exhibits a decrease after a maximum is reached, as typically shown in Figure 9(c) for the case of $T_c = -30^\circ$ at all λ values. The intriguing phenomenon, as pointed out previously, will be discussed later in detail in conjunction with Figure 16. To characterize the kinetics of the crystallization, we can approximately estimate $t_{1/2}$ for the crystallization from Q_r versus t, as shown in the inset of Figure 10. As shown in Figure 10, $t_{1/2}$ at a given λ value decreases as T_c is lowered, and that at a given T_c value decreases with λ. The latter effect is more pronounced at higher T_c values. In other words, the effect of the orientation on the crystallization rate is more pronounced at lower supercoolings.

Changes in the crystallinity with time, as evaluated from the changes in the WAXS profiles with time as demonstrated earlier in Figure 5, are, in turn, presented in Figure 11. X_c for a given λ value of 2.0 [Fig. 11(a)] shows that crystallization occurs faster at lower

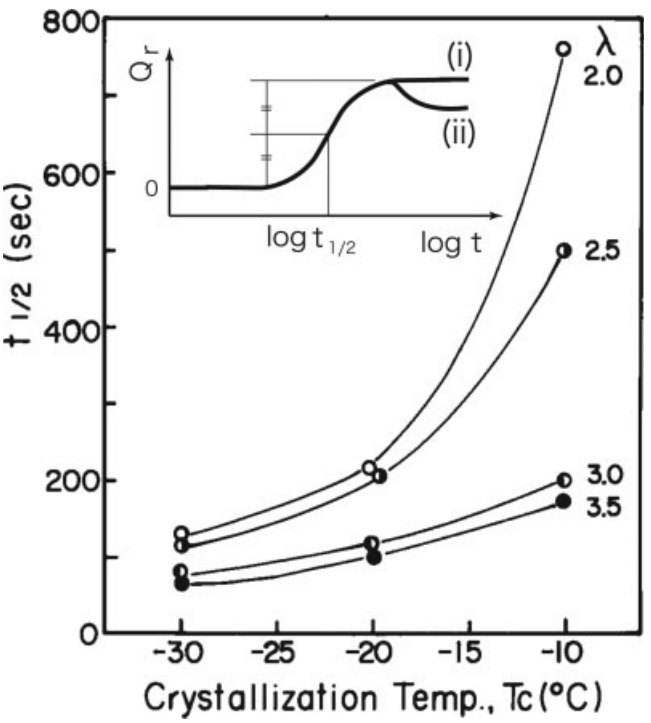

Figure 10 $t_{1/2}$ of isothermal crystallization measured from Q_r versus t (as shown in Fig. 9) as a function of T_c and λ. The inset shows the definition of $t_{1/2}$ for cases i and ii, in which Q_r increases with time without and with overshooting, respectively. Case ii underestimates the value $t_{1/2}$, although the error is not significant in the analyses given in the text.

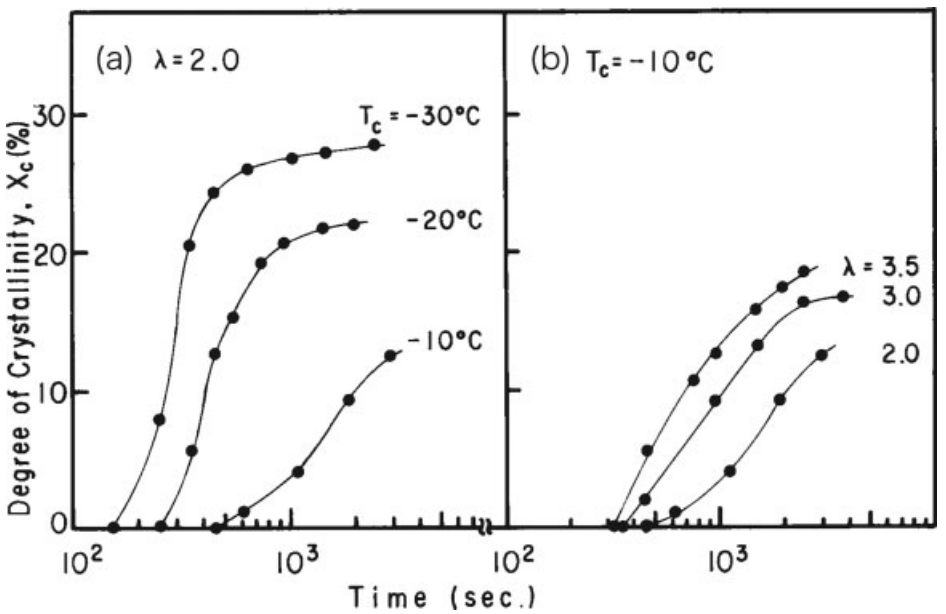

Figure 11 Changes in the crystallinity determined from WAXS as functions of time for (a) the samples elongated to $\lambda = 2.0$ and crystallized at various T_c values and (b) the samples crystallized at $T_c = -10^\circ$C and elongated to various λ values.

T_c values, also reaching a higher degree of crystallinity. A comparison of crystallizations occurring at the same temperature ($T_c = -10^\circ$C) but at various λ values [Fig. 11(b)] implies that the larger λ is, the faster the crystallization rate is and the higher the crystallinity is. Crystallization occurring in the sample having low-to-intermediate orientations occurs more slowly than that in the samples exhibiting higher orientation, as later discussed in conjunction with Figures 13, 14, and 18.

Figure 12 compares curves of the reduced stress relaxation measured during the crystallization of samples at fixed elongations of $\lambda = 2.0$ and $\lambda = 3.0$ and at various T_c values; σ and σ_0 are the stress at a given time t after the onset of crystallization and the stress at $t = 0$, respectively. In both cases, the more pronounced and faster relaxation is observed at a lower value of T_c. The data clearly indicate that stress relaxation occurs as a result of the progress of the crystallization with time.

High orientations

We classified the oriented crystallization at the fixed λ value of 4.5 and at $T_c = -30$ to $+10^\circ$C as crystallization under high orientations.

In the previous section, we present and discuss the effects of the crystallization conditions given by the sets of λ and T_c on each of the structural parameters separately. Because a general trend concerning the effects of λ and T_c on each parameter has been more or less clarified, we present here our results from a viewpoint different from that in the previous section. That is, we present the effects of isothermal crystallization under high orientations from the viewpoint of how the time evolutions of structural parameters $L(t)$, $Q_r(t)$, and $X_c(t)$ as well as stress relaxation $\sigma(t)$ are correlated to one another under given crystallization conditions (λ and T_c).

Typical SAXS profiles measured as a function of time under a high draw ratio of $\lambda = 4.5$ have already been demonstrated in Figure 3(a,b). The time dependence of L and Q_r has been determined from such data

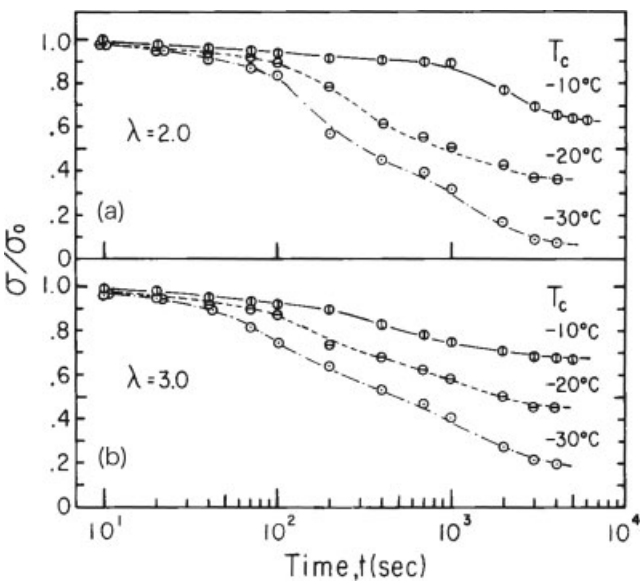

Figure 12 Stress relaxation during isothermal crystallization at various T_c values for the samples elongated to λ values of (a) 2.0 and (b) 3.0.

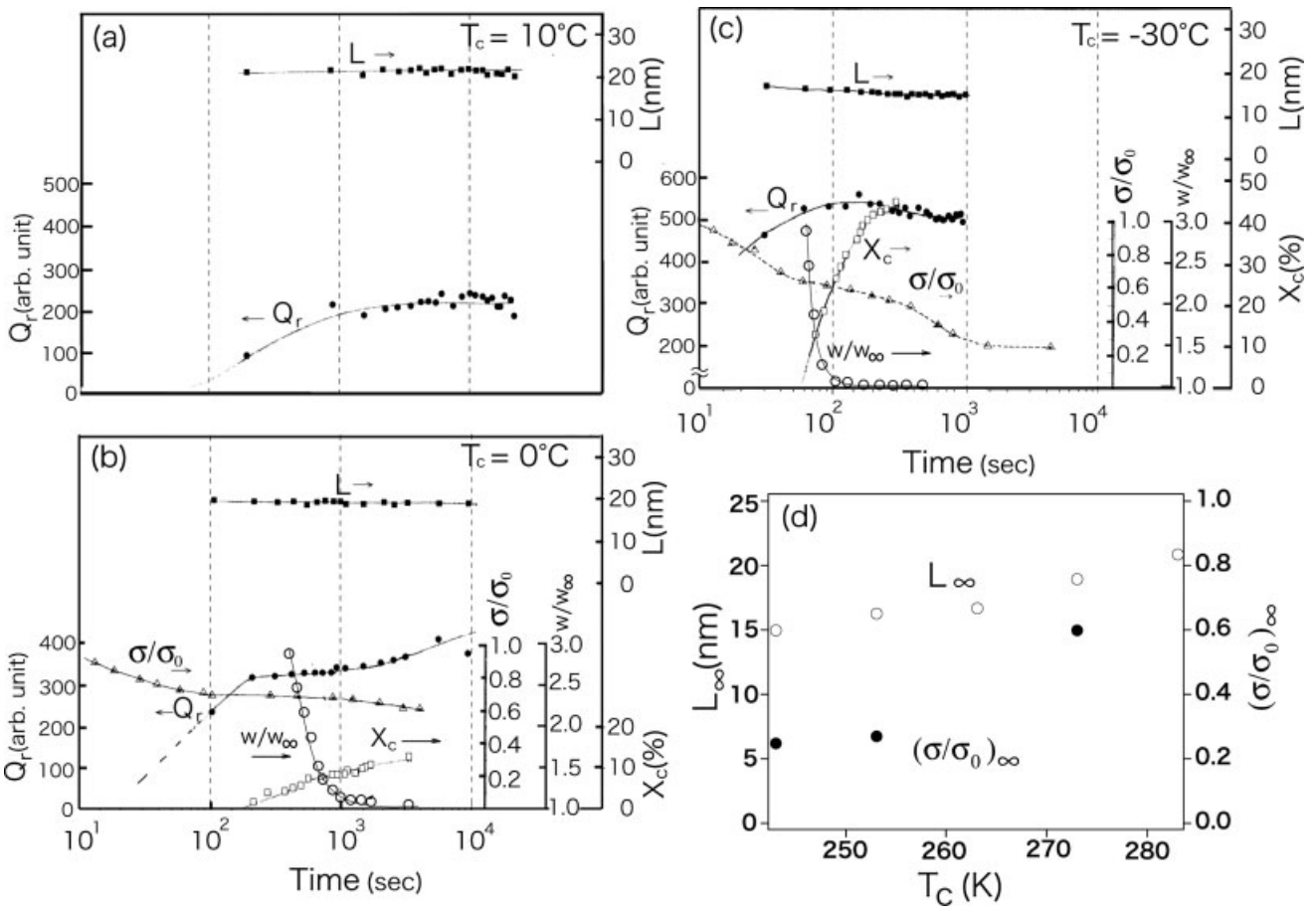

Figure 13 Time evolution of the structural parameters during isothermal crystallization for samples elongated to $\lambda = 4.5$ at various T_c values: (a) +10, (b) 0, and (c) −30°C. Part d shows L_∞ and $(\sigma/\sigma_0)_\infty$ at the long time limit of the isothermal crystallization.

obtained for a number of T_c values. WAXS profiles demonstrated earlier in Figure 5(b) show that X_c of the sample elongated to $\lambda = 4.5$ and crystallized at $T_c = 0$°C develops gradually with time, starting from approximately 200 s. Changes in the structural characteristics observed during the crystallization of the samples elongated to $\lambda = 4.5$ and crystallized at various T_c values are summarized in Figure 13(a–c). Before we go into a detailed discussion, the following intriguing points are worth being noted: (1) the SAXS maximum corresponding to L appears very early in the crystallization process, as shown in Figure 13(c), and (2) the decrease in L with time, as found in weak-to-intermediate orientations, is less pronounced.

Figure 13(a) demonstrates structural changes at $T_c = +10$°C. This temperature is higher than the nominal T_m value of ~ -3°C at $\lambda = 1$. The crystallization occurs very slowly at this temperature, and practically only changes in SAXS are observed; that is, WAXS hardly shows diffraction peaks due to crystal formation. Under such conditions, L appears to be constant during the whole process since the initial instant of time at which it can be observed. In contrast, Q_r (SAXS) gradually increases with time till a saturation level is reached. It can be postulated therefore that the periodicity of the structure (more rigorously a periodic electron density fluctuation) is formed much earlier before the final Q_r value is achieved. Also, it can be concluded that crystallinity that develops during the process is low or the crystals that form are imperfect, although SAXS has revealed some ordering at a larger length scale. This intriguing phenomenon is discussed in detail later.

Figure 13(b), in turn, shows changes in the characteristic parameters measured during crystallization at $T_c = 0$°C again for the sample elongated to $\lambda = 4.5$. In this case, changes in both WAXS and SAXS scattering can be observed. The relaxation of the reduced stress (σ/σ_0) can be observed from the early stage of the ordering process, whereas other characteristic parameters can be measured only after some time. Therefore, the stress relaxation appears to occur as a result of ordering, as revealed by an increase in Q_r, which may be called precrystallization ordering in the sense that Q_r increases but X_c does not yet clearly appear. At this temperature, Q_r (SAXS) appears earlier than X_c (WAXS). This finding is discussed in detail later. Here also, L is constant, starting from the early stage after

the instant of time at which it can be measured. Q_r also behaves in a manner similar to that for the case of $T_c = 10°C$, showing an increase at the beginning followed by leveling off. In contrast to the case at 10°C, Q_r at 0°C shows a secondary increase. The secondary increase of Q_r appears to occur parallel to the secondary relaxation of the stress. The reduced integral width of the (020) diffraction [w/w_∞, where w and w_∞ are the integral widths of the (020) diffraction at a given time t and at the long time limit after the onset of the crystallization, respectively] shows a remarkable decrease almost concurrently with the increase in X_c and a leveling off also when X_c (WAXS) tends to level off.

Behavior similar to that shown in Figure 13(b) can be observed at $T_c = -30°C$ in Figure 13(c). Here again, L hardly changes during the crystallization. Q_r (SAXS) clearly shows the same overshoot as shown in Figure 9(b,c), showing a decrease after reaching a maximum. The time evolution of X_c (WAXS) shows a substantial delay with respect to that of Q_r (SAXS) and reaches saturation when Q_r starts to decrease. The crystallization process, as revealed by changes in X_c and Q_r versus t, is accompanied by stress relaxation, showing rapid relaxation during precrystallization (ordering process where Q_r increases), followed by slow relaxation during the crystallization process in which X_c increases and eventually by the final stage of rapid relaxation after Q_r and X_c reach saturation, which may be interpreted as a result of the secondary crystallization process. An initial increase in X_c (WAXS) is also accompanied by a rapid decrease in w/w_∞.

Figure 13(d) shows both L and σ/σ_0 at the long time limit, which are defined as L_∞ and $(\sigma/\sigma_0)_\infty$, respectively, as a function of T_c for the isothermal crystallization process at $\lambda = 4.5$. As the degree of supercooling is increased, L_∞ decreases, which is reasonable in terms of an increase in the bulk free energy reduction of crystallization against the interface free energy cost. The decrease in $(\sigma/\sigma_0)_\infty$ with decreasing T_c is also reasonable as X_c increases with decreasing T_c.

Comparison of the effects of oriented crystallization under weak-to-intermediate orientations and high orientations on the time evolution of the structures

We discuss here the effects of varying the degree of network-chain orientations on the time evolutions of various structural parameters [$L(t)$, $Q_r(t)$, and $X_c(t)$] as well as the reduced stress relaxation [$\sigma(t)/\sigma_0$] in comparison with the isothermal crystallization for the corresponding unoriented system, which is used as a reference.

Weak-to-intermediate orientations

Although in an earlier section we discuss how the time evolution of each structural parameter [$L(t)$, $D(t)$, $Q_r(t)$, and $X_c(t)$] as well as $\sigma(t)$ depends on the various crystallization conditions (λ and T_c), we discuss here how the time evolutions of various structural parameters and that of $\sigma(t)/\sigma_0$ correlate under each given crystallization condition (λ and T_c).

Figure 14 summarizes the changes in the various characteristic parameters during crystallization at low-to-intermediate orientations and at T_c values of -10 and $-30°C$. Figure 14(a) shows the parameters determined for the sample elongated to $\lambda = 2.0$ and crystallized at $-10°C$. D, determined from the Guinier

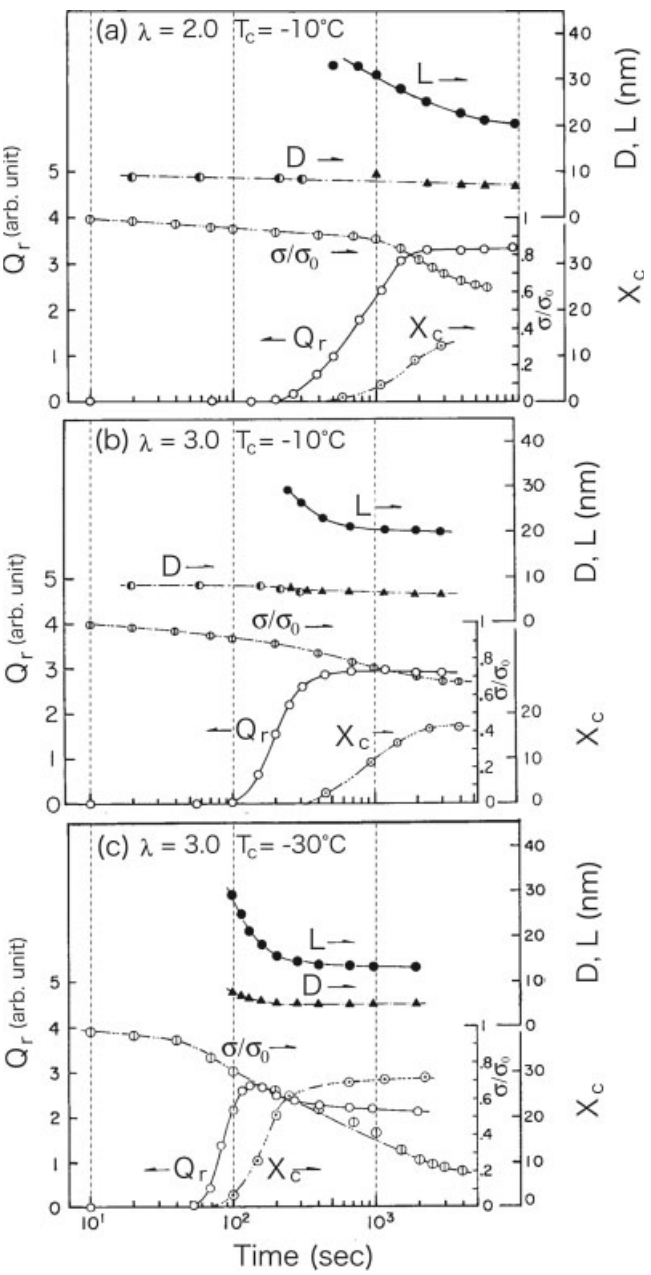

Figure 14 Time evolution of structural parameters L, D, Q_r, and X_c as well as σ/σ_0 during isothermal crystallization: (a) at $T_c = -10°C$ and $\lambda = 2.0$, (b) at $T_c = -10°C$ and $\lambda = 3.0$, and (c) at $T_c = -30°C$ and $\lambda = 3.0$.

plot at the beginning of the crystallization process, well coincides with that determined from the one-dimensional correlation function at the later stage of the crystallization process. Moreover, in the whole range of the process, D essentially remains constant, whereas L decreases with the crystallization time. It is also evident that Q_r (SAXS) increases much earlier than X_c (WAXS). The relaxation of the stress in this case [Fig. 14(a)] better correlates with the crystallization process revealed by X_c (WAXS) and with changes in L than with the changes in Q_r (SAXS), the behavior of which is different from the case of high orientations [see Fig. 13(b,c)].

Similar changes, except for a shift in the timescale toward a shorter timescale where L, σ/σ_0, Q_r, and X_c change, are visible in the plot presented in Figure 14(b), which presents data for the sample elongated to $\lambda = 3.0$ and crystallized at -10°C. Here again, D remains almost constant during the whole process, whereas L decreases. The saturations of L and Q_r occur practically at the same time. The WAXS crystallinity increases much later than Q_r, as in the case of Figure 14(a). The relaxation of the stress also occurs in parallel to the increase in X_c.

Slightly different behavior can be observed in the sample elongated to $\lambda = 3.0$ and crystallized at -30°C [Fig. 14(c)] in the following points. First, both D and L decrease with the crystallization time, although the decrease in D is much less than that in L. The small decrease in D may be due to internal ordering of crystals, which involves densification and hence a thinning of D. Second, Q_r increases to a maximum value and then decreases, whereas X_c increases with time, reaches saturation, and remains constant. Third, the relaxation of stress in this case is more pronounced than that observed in the case shown in Figure 14(a,b). The increase in Q_r also contributes to the stress relaxation in this case. The delay of the time evolution between Q_r and X_c is found in this case, too. However, the delay decreases with decreasing T_c from -10 to -30°C.

These results indicate that the time evolutions of the characteristic parameters during the crystallization process show qualitatively and quantitatively different behaviors when λ and T_c are changed within the range of the weak-to-intermediate orientations. Nevertheless, we can find some common trends in this region when we compare the trends with those in other ranges of deformations (i.e., under high orientations and no orientation, as detailed later). We summarize below some universal features found in the ordering process encountered in the weak-to-intermediate orientations in Figure 15. Figure 15(a) shows schematically the kinetics of the crystallization, as observed by time evolutions of L, D, Q_r, X_c, and σ, and Figure 15(b) shows schematically the time evolutions of the spatial electron density profile. Those trends are

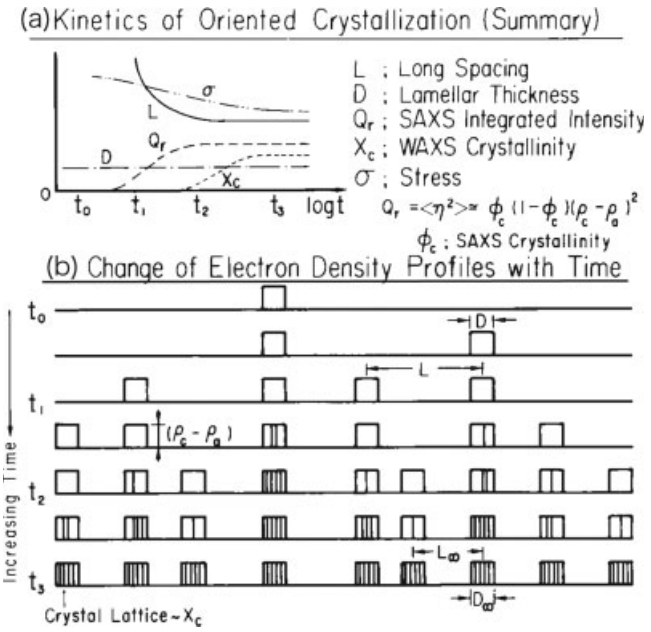

Figure 15 Schematic model describing the time evolution of the structures for isothermal crystallization under weak-to-intermediate orientations that could be responsible for the observed behavior of SAXS (L, D, and Q_r), WAXS (X_c), and σ. ϕ_c in part a corresponds to ϕ_c given by eq. (5) in the text, which defines the local crystallinity given by D/L.

well interpreted in the context of nucleation and growth processes for the oriented crystallization of the network chains.

The differences in the time evolution of Q_r (SAXS) and X_c (WAXS) are especially remarkable. The observed changes in Q_r and X_c with time suggest that in a very early stage of crystallization (t_0 to t_1 in the figure), lamellar crystallites of thickness D are nucleated randomly in space, forming an irregularly spaced, one-dimensional array along the elongation direction [horizontal axis in Fig. 15(b)], as seemingly evidenced by such a process leading to an increase in the electron density fluctuations, as observed by an increase in Q_r. However, the number of lamellae is still too small to give rise to the SAXS maximum, which reflects L. D is kept constant with time, although it depends on T_c and λ. It is conceivable that the electron density difference between more ordered regions and the less ordered matrix (i.e., the height of the box with width D) is increasing with time, although the model ignores this for the sake of simplicity. The perfection of crystal lattice in lamellae, which is schematically illustrated by a number of lines within the lamellae (the larger the number is, the more perfect the lamellar crystals are), is at this stage so poor that X_c (WAXS) cannot be measured.

As time elapses, the number of lamellae increases, giving rise to a well-defined value of L, which decreases with time (from t_1 to t_2). The increase in Q_r

accompanies the decrease in L and hence increase in ϕ_c toward 1/2. The time dependence of Q_r and L levels off to some constant values defined by $Q_{r,\infty}$ and L_∞. Obviously, this time at which $Q_{r,\infty}$ and L_∞ are attained should correspond to the time (t_2) at which the number of lamellae also reaches a constant value. The fact that Q_r develops much earlier than X_c indicates that the ordering on a larger scale, as evidenced by the occurrence of periodic density fluctuations, occurs earlier than the ordering on a local scale, as evidenced by the formation of a crystal lattice structure. Lamellae in the early stage of the phase transition (from t_0 to t_1) exhibit a higher density than the amorphous surroundings but do not have well-developed crystal lattices. Stacks of such lamellae could contribute to Q_r (SAXS) without a significant contribution to X_c (WAXS). The perfection of the crystal lattice is improved in the time domain from t_2 to t_3 through local rearrangements of the molecules within the defected lamellar crystals, which are already arranged into periodic arrays responsible for L. Consequently, the ordering process first fixes the large length-scale periodic structures and then the local crystal-lattice structure. This unique ordering process may be attributed to long-range interactions (or strong correlations) of network chains along the elongation direction enhanced by the stretching of the sample.

One of the intriguing observations made during crystallization at -30°C for the sample elongated by $\lambda = 3.0$ is a decrease in Q_r (SAXS) at a later stage of crystallization ($t > t_1$ in Fig. 15), even though that the overall WAXS crystallinity is low ($X_c \leq 30\%$). This can be explained by the model presented in Figure 16. The model assumes the occurrence of a number of crystallizing grains comprising lamellar stacks in an amorphous matrix. The grains themselves separate from one another by such a large distance that no intergrain interference comes into play in the SAXS q range covered in the experiments. In such a case, only the sum of independent scattering intensity from the individual grains is important. The crystallinity of such grains might be higher than X_c averaged over the volume, which is detected by WAXS. The crystallization may occur by filling gaps between lamellae with newly developed lamellae inside the grains, as schematically illustrated by a change in the internal structure of the grain from Figure 16(a) to Figure 16(b). If this is the case, Q_r depends on the local crystallinity in the grain ($X_{c,g}$) rather than X_c averaged over the whole sample volume. When $X_{c,g}$ exceeds 0.5, the overshooting of Q_r should be observed, as Q_r in this case is given by

$$Q_r \propto X_{c,g}(1 - X_{c,g})(\rho_c - \rho_a)^2 \quad (9)$$

The stress relaxation might be due to two mechanisms. The first is slippage of those entangled macromolecules that are connected to different network

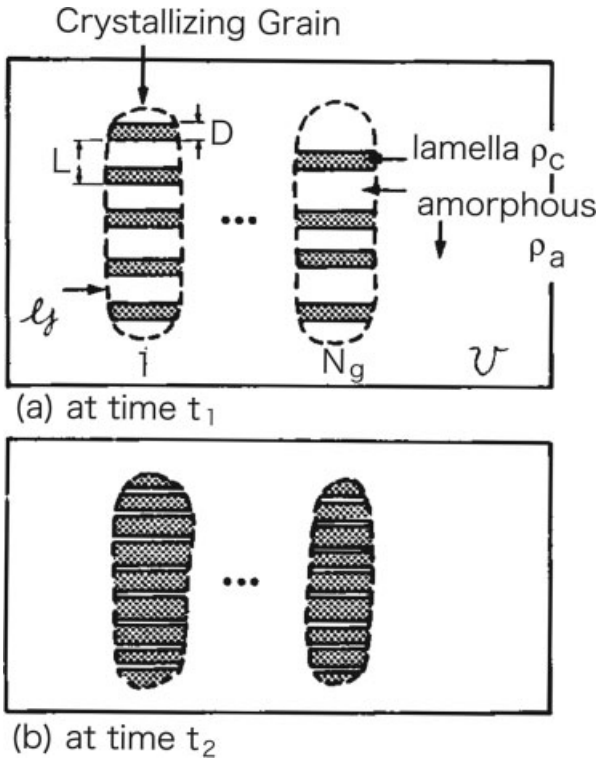

Figure 16 Model describing an overshoot of Q_r (SAXS) during the isothermal crystallization of the samples. The model assumes a superstructure consisting of a number of crystallizing grains (N_g) in the amorphous matrix. The local crystallinity (given by D/L) within the grains may increase with time (from t_1 to t_2 in Fig. 15) and may exceed 1/2 at $t > t_2$, depending on the crystallization conditions.

points of the crosslinked polymer. The second mechanism is the relaxation of network chains due to crystallization into extended-chain crystals or folded-chain lamellar crystals. In the molten stretched network chains, the former is the only mechanism for stress relaxation before the system attains an equilibrium stress. However, under the conditions in which crystallization occurs in the stretched network, the crystallization makes a dominant contribution to the stress relaxation, as crystallization into chain-folded lamellae[13] or bundle-type, extended-chain crystals[37,38] involves relaxation of stretched network chains.

The following remarks are worth being noted. In the case of the oriented crystallization of network chains into chain-folding lamellae, the crystallization may involve first stress relaxation and then a stress increase upon further crystallization[13,22,37] because keeping the process of intrachain folding of the network chains into lamellae during crystallization may involve stretching of the rest of the network chains that are not yet incorporated into crystals. This increase in the stress, however, may depend on crystallization conditions λ and T_c. We have never observed an increase in the stress during crystallization under our experimental conditions of weak-to-in-

termediate orientations or high orientations. The lack of an increase might have resulted from the crystallization of less stressed chains or free-end chains of the networks into folded-chain crystals.

High orientations

Crystallization under high orientations exhibits characteristics for spinodal-like crystallization. We clarify these characteristics next.

During crystallization at high orientations [e.g., at $\lambda = 4.5$ and $T_c = -30^\circ$C, as in the case of Fig. 13(c)], the time lag between the evolution of X_c (WAXS) and that of invariant Q_r (SAXS) is generally much larger than that observed at the smaller orientations [cf. Fig. 14(c) at $\lambda = 3.0$ and $T_c = -30^\circ$C]. During the time in which Q_r increases and reaches almost a constant value, X_c still gradually increases. L reaches a constant value at a very early time. This means that the large length-scale density fluctuations (kinds of ordered structures), as observed by SAXS, are formed much earlier than the local order (crystal lattice) detected by changes in WAXS.

It can be generally concluded that in the highly oriented systems crystallization occurs in such a manner that (1) a large length-scale structural frame such as density fluctuations with a fixed spacing L is first built up and (2) this process is followed by a gradual shaping-up of the internal fine structure. The former process involves an increase in the amplitude of density fluctuations, as revealed by an increase in Q_r at a fixed value of L. This is typically the case for the results shown in Figure 13(a). The latter process involves the perfection of the crystal lattice, as observed by an increase in X_c and a decrease in w/w_∞, as typically found in the results shown in Figure 13(b,c). This early stage of the ordering process resembles the well-known process of spinodal decomposition,[39–41] in which binary mixtures decompose to form periodic composition fluctuations, with their amplitude gradually increasing with time. This system at $T_c = 10^\circ$C [Fig. 13(a)] is interpreted to involve spinodal decomposition of noncrystallizable parts (crosslinked points) and crystallizable parts (linear chains between the crosslinks) of the molten, crosslinked network chains. The instability of the molten network chains is driven by a high degree of chain orientations and by orientation-induced crystallization of crystallizable linear chains; the periodicity L of the density fluctuations and saturations of the increasing amplitude of the fluctuations as revealed by Q_r vs t are expected to be controlled by crosslinking.

When crystallization obviously occurs, as in the cases shown in Figure 13(b,c), because of the larger supercoolings, highly defected crystallites are first formed in the regions rich in crystallizable parts, and then defects gradually segregate, giving rise to the growth of the amplitude of the density fluctuations with time. Such a process is called spinodal crystallization.[33,42,43] Here the pioneering works reported in refs. 42 and 43 are concerned with spinodal crystallization for drawn linear polypropylene melts. Kaji and coworkers[44,45] extensively studied spinodal crystallization from polymer melts that were uncrosslinked and unoriented. A theory presenting one of the possible mechanisms for such a process was recently developed by Olmstead et al.[46] and Ryan et al.[47] Earlier works by Petermann and coworkers,[42,43] subsequent works by Kaji and coworkers,[44,45] and the works by Ryan et al.[47] are all concerned with the spinodal crystallization of uncrosslinked polymer melts. On the contrary, this work and the preceding work[33] are unique, in that they deal with highly oriented, crosslinked polymer melts. However, in normal cases of spinodal decomposition for binary mixtures, a coarsening process occurs, causing further growth of composition fluctuations with respect to both the amplitude of the fluctuations and the characteristic size.[40,41] In this case, the existence of crosslinking points and/or the occurrence of crystallization prevents further growth of fluctuations, causing freezing-in of the coarsening processes. This kind of freezing due to crystallization has also been observed in other crystallizable binary systems.[48]

The evolution of Q_r exhibits an overshoot, that is, a maximum even at a relatively low crystallinity (<0.5), as measured by WAXS. This indicates that most likely the crystalline superstructure having the grains separated in the amorphous matrix is developed, as already discussed and shown in Figure 16. However, the overshoot is much less remarkable in the case of high orientations than in the case of weak-to-intermediate orientations.

Figure 17 shows the time evolution of the scattering parameters for unoriented crystallization for reference for the oriented crystallization. The SAXS intensity maximum corresponding to L during crystallization at -30°C is very weak and appears at ~ 700 s after the sample is cooled to T_c, although the SAXS profile is not shown here. The WAXS profiles also develop at some time after the crystallization, although they are not shown in this article. As shown in Figure 17(b), Q_r (SAXS) changes according to a well-defined sigmoidal curve. Those changes are closely accompanied by changes in X_c (WAXS). L, measured from the SAXS maximum, decreases during the whole time of the crystallization. Very similar behavior can be observed at $T_c = -20^\circ$C in Figure 17(a). An increase in Q_r can also be observed during crystallization at -50°C [Fig. 17(c)]. This increase is followed by saturation at some level. Simultaneously, L slightly decreases, whereas Q_r is increasing. It reaches a constant value when Q_r does so. X_c (WAXS) could not be measured, simply because well-defined diffraction profiles could not be observed

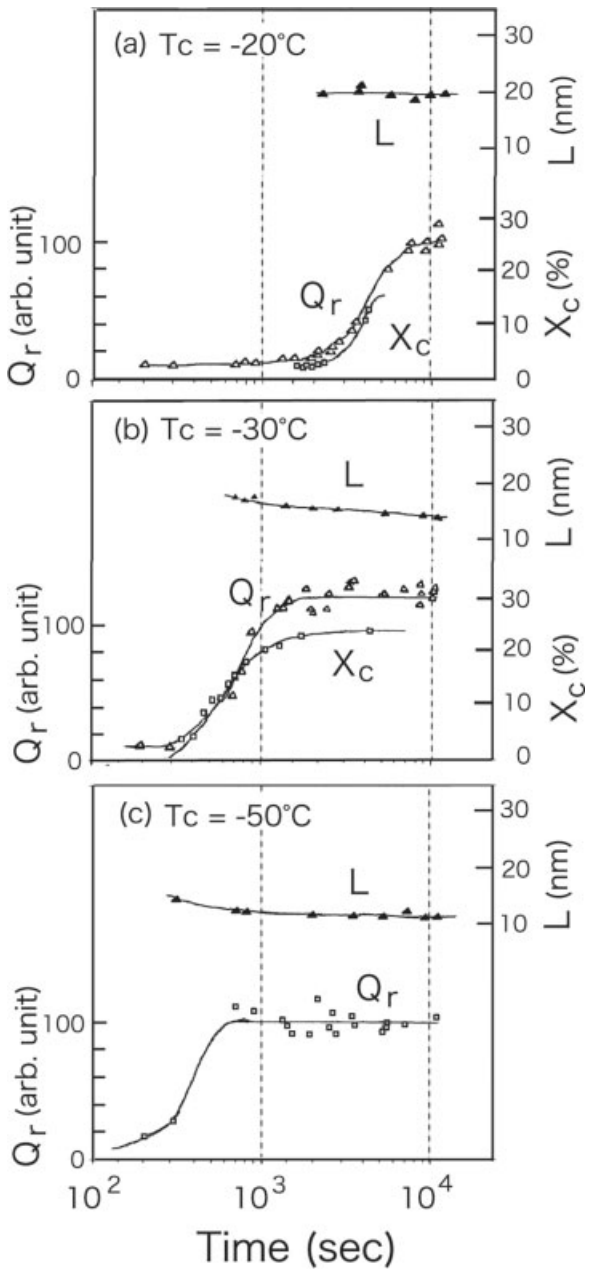

Figure 17 Time evolution of the structural parameters during isothermal crystallization for undeformed samples crystallized at various temperatures: (a) −20, (b) −30, and (c) −50°C.

in the timescale covered in this experiment. This is probably because the rate of formation of the crystal lattice is very slow at $T_c = -50°C$.

A comparison of the $t_{1/2}$ values for undeformed samples ($\lambda = 1$) and for highly elongated samples ($\lambda = 4.5$) is shown in Figure 18. $t_{1/2}$ was determined from $X_c(t)$ and defined in a manner similar to the case shown in the inset of Figure 10. The figure also includes the $t_{1/2}$ values evaluated by SAXS and WAXS at $\lambda = 2$ (typical for the case of weak-to-moderate orientations) for reference. The orientation-induced crystallization causes a very pronounced increase in the crystallization rate (a decrease in $t_{1/2}$ measured at the given T_c values). T_c itself also shows a strong effect on the crystallization rate, which increases with a decrease in T_c. In the case of undeformed samples, $t_{1/2}$, measured by means of WAXS, can be observed to coincide with $t_{1/2}$ measured by SAXS at $T_c \geq -30°C$, whereas in the highly oriented samples with $\lambda = 4.5$, the coincidence is observed only at $T_c > -10°C$. A time lag between SAXS and WAXS data is remarkably enhanced in highly oriented samples and can be observed at $-30°C \leq T_c < -10°C$. The lower the temperature is, the more pronounced the time lag is. The time lag between $t_{1/2}$ as observed by Q_r (SAXS) and $t_{1/2}$ as observed by X_c (WAXS) may be interpreted as follows.

The SAXS $t_{1/2}$ value reflects the large-scale periodic structure associated with L, whereas the WAXS $t_{1/2}$ value reflects the short-scale structure associated with the formation of the crystallites and crystal lattice. At low T_c values, at which the systems have large supercoolings, the thermal fluctuation effects[49] on the periodic density fluctuations are small, so the systems have a large correlation length inherent in the thermodynamic state of the systems. In this situation, the large-scale structure is first built up, and this is followed by the buildup of the local-scale crystal structure and by the improvement of the lattice perfection. On the other hand, at high T_c values, the effects of the thermal fluctuations are enhanced, and they reduce the correlation length of the large-scale density fluctuations. This effect, in turn, causes an evolution of the large-scale structures as a result of the evolution of the

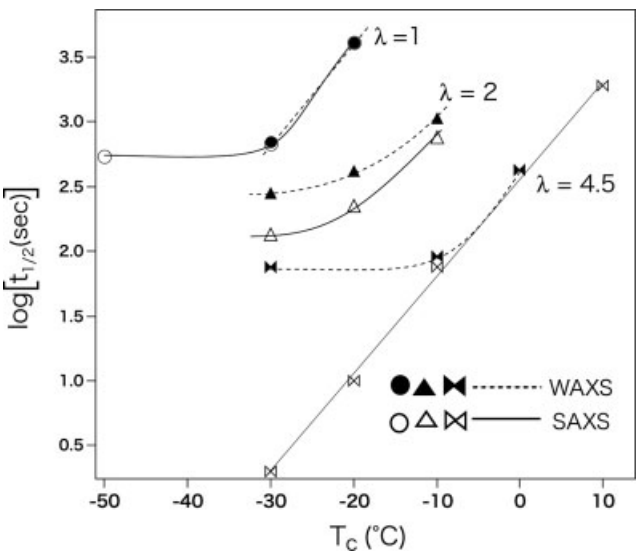

Figure 18 $t_{1/2}$ determined from the time changes in Q_r (SAXS) and X_c (WAXS) for the undeformed samples ($\lambda = 1.0$), weakly-to-intermediately oriented samples ($\lambda = 2.0$), and highly oriented samples ($\lambda = 4.5$). The $t_{1/2}$ values for SAXS and WAXS are shown by solid and dotted lines, respectively.

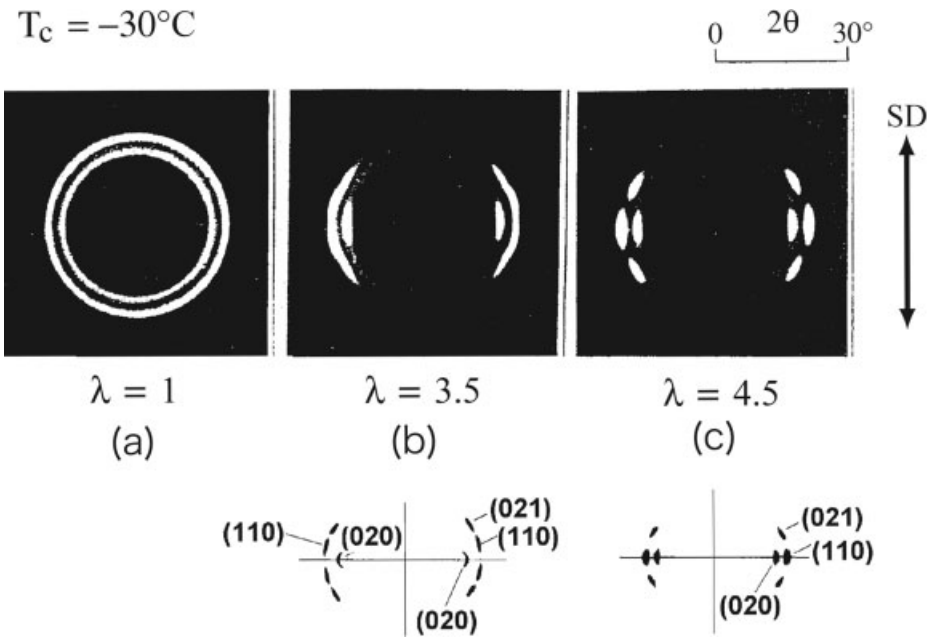

Figure 19 Photographic WAXS patterns for samples at (a) $\lambda = 1.0$, (b) $\lambda = 3.5$, and (c) $\lambda = 4.5$. All were crystallized at $-30°C$.

short-scale structures and hence causes the SAXS and WAXS $t_{1/2}$ values to be approximately equal. The larger λ is, the larger the effective supercooling is, and hence the smaller the thermal fluctuation effects are. This accounts for the experimental results showing an increasing time lag with decreasing T_c for the oriented crystallization, especially under high orientations of $\lambda = 4.5$.

Crystal texture

Figure 19 presents typical WAXS patterns crystallized at $T_c = -30°C$ for the samples elongated to various degrees before crystallization. The pattern from the undeformed material ($\lambda = 1$) shows a diffraction intensity independent of ψ, whereas anisotropic diffraction patterns are obtained for the elongated samples ($\lambda = 3.5$ and 4.5). At $\lambda = 3.5$, the (020) reflection, arising from the (010) crystallographic plane parallel to the c axis of the unit cell, appears along the equator, and the (110) diffraction is split with respect to the equator. The orientation distribution functions of the (110) and (020) reciprocal lattice vectors have been analyzed,[34] and the results indicate that the observed distribution functions can be explained on the basis of an orientation distribution of the lamellar crystals with the chain axis (c axis) tilted to the lamellar normal.

This picture changes at the elongation of $\lambda = 4.5$, at which both reflections, (020) and (110), are located on the equator, and consequently, the *c* axis is really parallel to the direction of elongation. This phenomenon might result from the change in the morphology of the growing crystals. That is, at the low elongation, crystallization occurs only in the form of lamellar crystals, whereas at the high elongation, the bundle-type, extended-chain crystals with the c axis oriented parallel to the elongation direction appear and become dominant over the chain-folded lamellae.

Figure 20(a–c) demonstrates the time evolution of the WAXS patterns, showing the intensity distribution along 2θ at $\psi = 90°$ (along the equator) (part a) and along ψ for the (020) diffraction (part b) and (110) diffraction (part c) during crystallization at $T_c = -30°C$ for the sample elongated to $\lambda = 4.0$. Figure 20(c) shows that the reflection from the (110) plane splits into the two reflections with their maxima at some angles with respect to the equator from the very initial moment of crystallization. Thus, the crystalline texture formed at $\lambda = 4.0$ seems to be the same as that at $\lambda = 3.5$. The angles of the maxima appear to increase with time to a saturated value.

Figure 21 shows the changes in the X-ray diffraction pattern during the heating of the sample, which was first crystallized at $T_c = -30°C$, under a constant elongation of $\lambda = 4.0$ toward 50°C at a rate of 1°C/min under the same fixed λ value of 4.0. An increase in the temperature causes a gradual melting of the crystalline texture that developed under the oriented crystallization. The melting process results in a decrease in the intensity of the equatorial reflection of (020), as shown in Figure 21(a–c). A decreased intensity of the split (110) reflections can be simultaneously observed, as shown in Figure 21(d,e). However, at +20°C, only a weak equatorial maximum corresponding to the (110) reflection remains, as shown in Figure 21(f). This means that some unmelted crystals with almost per-

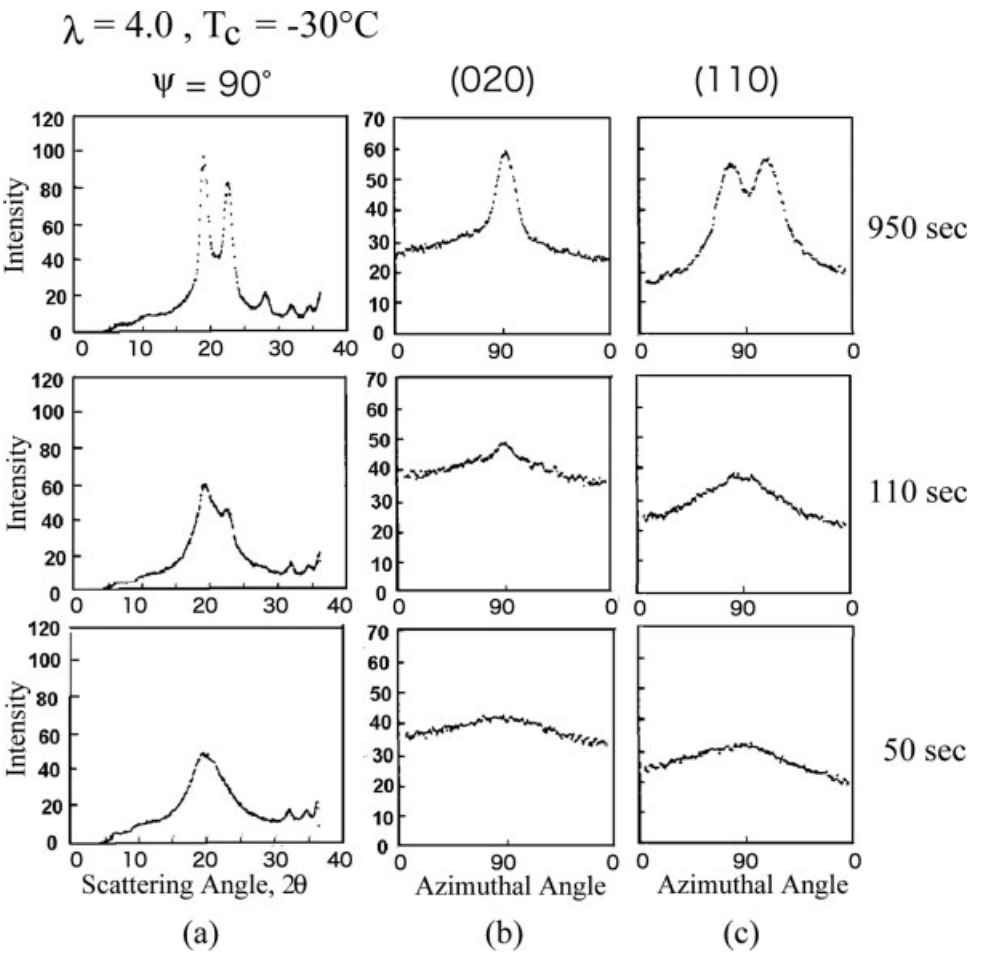

Figure 20 Time evolution of (a) equatorial WAXS ($\psi = 90^\circ$) and (b,c) the ψ dependence of the (020) diffraction and (110) diffraction, respectively, during isothermal crystallization at $T_c = -30^\circ$C for a sample elongated to $\lambda = 4.0$.

fect orientation for both (020) and (110) crystallographic planes still exist at this temperature, which is above the nominal T_m value of the specimen at $\lambda = 1$ (-3°C). Those crystals are anticipated to be most likely the bundle-type, extended-chain crystals developed under oriented crystallization, which will melt at higher temperatures than the folded-chain ones. The existence of the bundle-type, extended-chain crystals giving rise to the (110) diffraction maximum at the equator, as shown in Figure 21(f), is not clearly evidenced in Figure 20(c) during the isothermal crystallization process at $\lambda = 4.0$ and $T_c = -30^\circ$C. At least the following two possibilities may be suggested to explain this effect: (1) the signature of the extended-chain crystals might be hidden by the strong, split (110) diffractions and (2) the bundle-type, extended-chain crystals are formed only during the heating process under a constant λ value of 4.0 via molecular rearrangements through partial melting and recrystallization. At this moment, we cannot predict which case is more probable, and hence we shall leave this problem for future works.

The temperature at which the X-ray diffraction pattern disappears can be used as a method to determine T_m of the crystalline phase. This method applied to the determination of T_m gave the results presented in Figure 22. T_m is strongly affected by λ. T_m sharply increases with λ across the boundary between weak-to-intermediate orientations and high orientations, that is, around $\lambda \cong 3.5$. The characteristic curve well corresponds to the data obtained for the crosslinked rubbers with other methods of evaluation.[50,51]

An increase in the temperature of the sample, already crystallized at a given value of T_c and at a constant λ value of 4.5, with the same constant value of λ being kept, also causes variations of the stress, as it causes changes in the WAXS pattern, as shown in Figure 21. Figure 23 presents changes in σ with the temperature for various samples at a constant value of $\lambda = 4.5$, which are first crystallized at $\lambda = 4.5$ and at various T_c values. When the temperature is raised above T_c, the stress increases, and this is obviously a process opposite of the stress relaxation observed during crystallization; the melting of crystals gives rise to an increase in the stress borne by crosslinked, molten network chains. Because changes in the stress may be primarily attributed to the orientation of network chains in the amorphous part, this behavior should be well

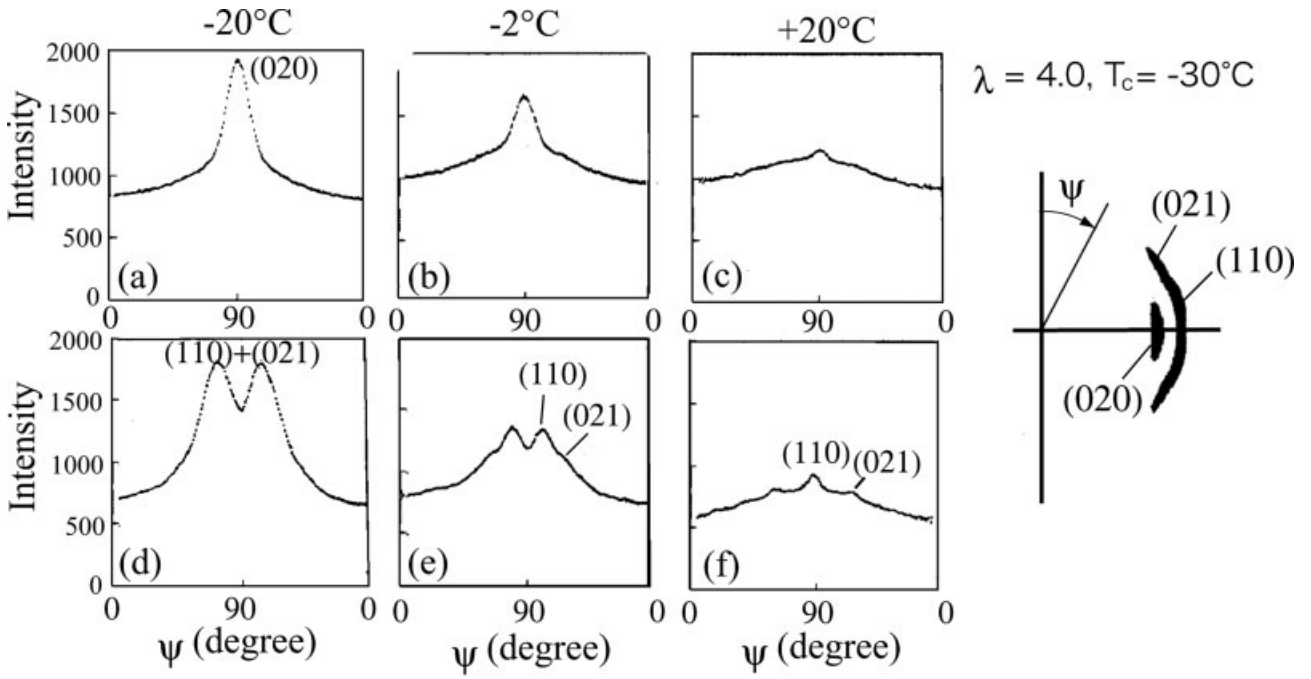

Figure 21 ψ dependence of (a–c) the (020) diffraction and (d–f) the (110) diffraction plus the (021) diffraction for the samples first subjected to isothermal crystallization at −30°C at a fixed λ value of 4.0 followed by an increase in the temperature to (a,d) −20, (b,e) −2, and (c,f) +20°C while λ is held constant at 4.0.

interpreted, at least qualitatively, on the basis of rubber elasticity theory,[52] which gives the following formula for the temperature dependence of stress in deformed, molten, crosslinked polymer chains:

$$\sigma \propto \nu kT\left(\lambda - \frac{1}{\lambda^2}\right) \tag{10}$$

where ν is the number density of the crosslinked, amorphous chains effective for the stress and λ is the effective elongation ratio of the crosslinked chains in the presence of crystals, k is the Boltzmann Constant and T is the absolute temperature.

Figure 23 shows discontinuous changes in the slope at some inflection temperature (T_f, marked by the arrow), slightly depending on T_c. The trend shown in Figure 23 does not change at all, even when σ/kT is plotted as a function of the temperature; this suggests that the trend reflects a change in $\nu(\lambda - 1/\lambda^2)$ with the temperature due to the melting of the crystals in the context of the theory given by eq. (10). The slope of the stress versus the temperature at temperatures lower than T_f is higher than that at temperatures higher than T_f. The difference is more pronounced for the samples crystallized at higher T_c values. The inflection point well coincides with changes in the X-ray diffraction pattern with the temperature, as already discussed in conjunction with Figure 21. It can, therefore, be postulated that the increase in σ up to T_f may be primarily due to the melting of folded-chain lamellar crystals. This can happen because the different molecules belonging to the same folded-chain crystal become free after a partial melting of the crystals. Most likely, the lower T_c is, the higher the content is of the folded-chain crystals with a smaller D_∞, and consequently the smaller the slope is of the stress–temperature curve. Above the inflection point, the bundle-type, extended-chain crystals may play a dominant role in σ versus the temperature. The bundle-type, extended-chain crystals melt at much higher temperatures at which the last trace of X-ray diffraction disappears, as shown by the arrow labeled T_m at the right edge of the figure.

Similar plots are presented in Figure 24, showing the stress that builds up upon the heating of the samples at constant lengths of λ = 2.0–4.5. Before the heating, the samples are crystallized at $T_c = -30$°C and at fixed λ values (2.0, 3.0, 4.0, and 4.5). In this case, the parts of the plots occurring directly below the inflection point, as discussed earlier, are parallel to one another. This might indicate similar contributions of melting of the folded-chain lamellar crystals for the samples crystallized at $T_c = -30$°C at the given λ values. T_f again coincides with the change in the X-ray diffraction pattern, as discussed earlier in conjunction with Figure 21 [a change from the set of diffraction profiles of Fig. 21(b,e) to the set of those of Fig. 21(c,f)], in the case of λ = 4.0 and λ = 4.5. However, T_f in the case of λ = 2.0 and λ = 3.0 is simply due to melting of the folded-chain lamellar crystals [reflecting the disappearance of the split (110) diffraction]. Therefore, the inflection points are marked with arrows labeled T_m. The inflection point generally increases with an increase in the elongation up to λ = 3,

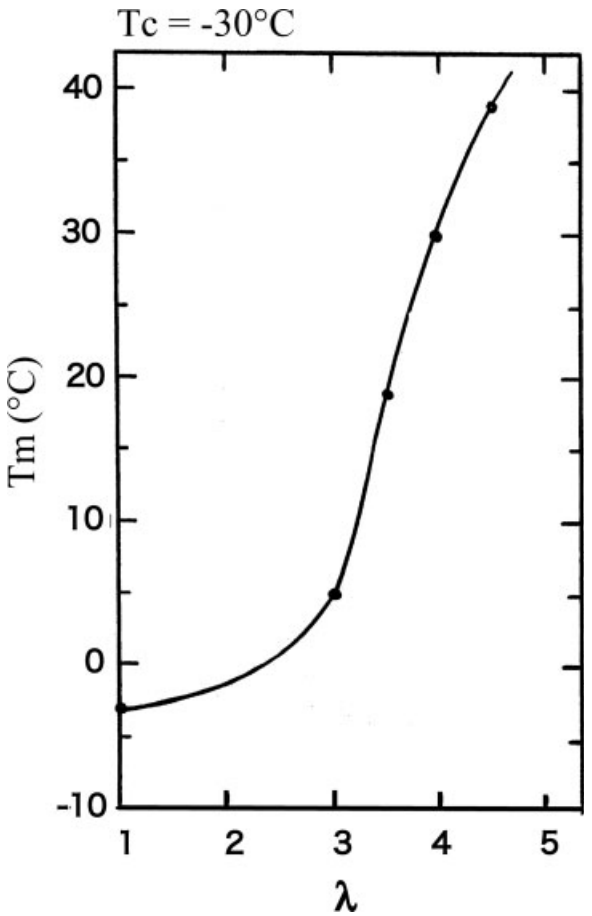

Figure 22 T_m versus λ as measured from the disappearance of the wide-angle X-ray diffraction pattern (as shown in Fig. 21).

and this is followed by a decrease upon a further increase in λ. At high elongations of λ = 4.0 and λ = 4.5, the X-ray diffraction pattern finally disappears at a much higher temperature than T_f, as shown by the arrows labeled T_m, because of the melting of the bundle-type, extended-chain crystals.

Avrami analysis

The conclusion concerning the occurrence of the bundle-type, extended-chain crystals in the samples crystallized at high elongations can be supported also by the kinetics of the crystallization process, which are analyzed by Avrami's theory:

$$x(t) = \exp\left\{-\left(\frac{t}{t_{1/2}}\right)^n \ln 2\right\} \tag{11}$$

n denotes Avrami's exponent:

$$n = m + i \tag{12}$$

m denotes the space dimension in which the crystals grow. i is assumed to be 1 for sporadic nucleation or 0 when nucleation is predetermined. $x(t) = 1 - X_c(t)$ is the weight fraction of the amorphous component.

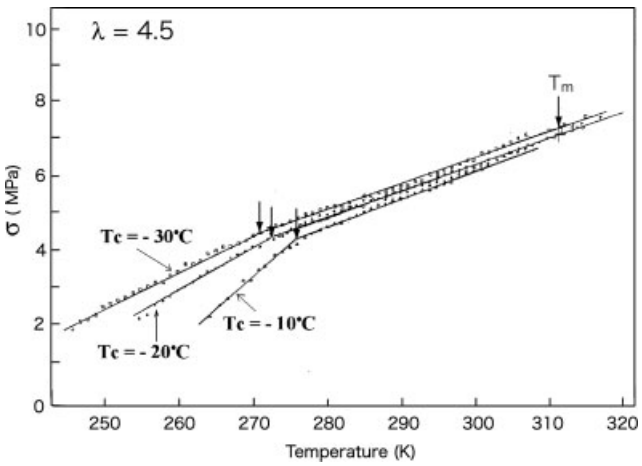

Figure 23 Stress recovery (σ) as a function of the temperature during the heating of samples at a constant length indicated by λ = 4.5. Before the heating, the samples were first subjected to isothermal crystallization at λ = 4.5 and at various T_c values. The arrows indicate the inflection points of the plot of σ versus the temperature.

The plots presented in Figure 25(a,b) show that n is close to 2 for the sample crystallized at a high elongation of λ = 4.5, whereas for an undeformed sample, n is 3. When homogeneous nucleation is assumed for both cases (i.e., $i = 1$), those values of n correspond to $m = 1$ for one-dimensional growth (the bundle-type, extended crystals) for the case of λ = 4.5 and to $m = 2$ for two-dimensional growth (chain-folded lamellar crystals) for the undeformed polymer. In a previous section, we have pointed out that the crystallization behavior at λ = 4.5 and $T_c = 0°C$ can be described on the basis of spinodal-like crystallization. At first sight, this appears to contradict the application of Avrami analysis to such a system. However, it may be still pos-

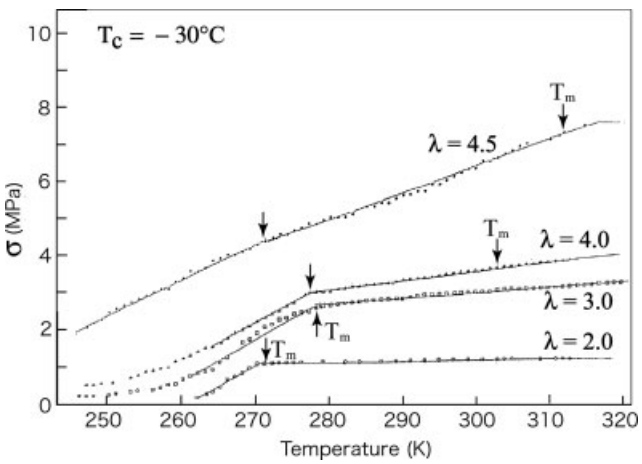

Figure 24 Stress recovery (σ) as a function of the temperature during the heating of samples at given constant lengths indicated by λ. Before the heating, the samples were first subjected to isothermal crystallization at $T_c = -30°C$ and at various λ values.

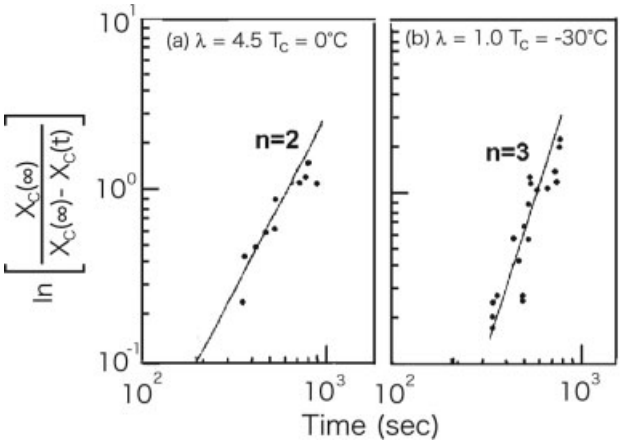

Figure 25 Avrami plots for (a) samples crystallized at $T_c = 0°C$ in a highly oriented state given by $\lambda = 4.5$ and (b) samples crystallized at $T_c = -30°C$ in an undeformed state. $X_c(t)$ and $X_c(\infty)$ are the WAXS crystallinities at a given time t and at the long time limit.

sible that the local crystallization in the region rich in the crystallizable component may proceed via the nucleation growth process.

CONCLUSIONS

SAXS and WAXS studies of the structural changes occurring during the oriented crystallization of crosslinked PB have been conducted in real time and accompanied by simultaneous measurements of the stress relaxation. The results reveal several peculiarities of the process. Photographic X-ray diffraction patterns (both WAXS and SAXS) demonstrate that even at low λ values, the final crystalline structure exhibits orientation of the crystal with respect to the elongation axis. From WAXS patterns, it can be concluded that the molecular axes in the crystal tend to orient along the elongation axis. The two-point SAXS patterns indicate the existence of regularly stacked lamellar crystals, with their lamellar normal oriented parallel to the stretching direction, although these points have not been explicitly emphasized in this work as the phenomena are well expected.

A gradual evolution of the wide-angle X-ray diffraction pattern can be used to evaluate the kinetics of crystallization in the system. Figure 18 shows that, in the range of $-50°C \leq T_c \leq 10°C$, the crystallization rate (proportional to the inverse of $t_{1/2}$) at a given λ value in the range of $2.0 \leq \lambda \leq 4.5$ increases with a decrease in T_c. At constant T_c values, the crystallization rate increases with an increase in λ. The values of $t_{1/2}$ obtained from SAXS are shorter than those measured by WAXS, as also shown in Figure 18 for $\lambda = 2.0$ and $\lambda = 4.5$ at low T_c values ($T_c < -10°C$), in contrast to the case of $\lambda = 1.0$, which tends to show no obvious difference down to $T_c = -30°C$. This means that ordering occurs first on the large length scale revealed by SAXS before the well-developed crystal structure, revealed by WAXS, is formed on the local scale. The time lag is greater for the larger supercoolings, a possible interpretation of which is proposed in conjunction with Figure 18.

In the weak-to-intermediate orientations, D remains practically constant during the course of crystallization, whereas L decreases with time (such an effect was also reported by Schultz at al.[2]); this occurs almost simultaneously with an increase in Q_r (Fig. 14). Crystallization under high orientations involves ordering induced by the instability of melts consisting of highly oriented amorphous chains, giving rise to periodic density fluctuations with almost time-independent periodicity (L) and a gradual evolution of the amplitude of the density fluctuations that is accompanied by subsequent crystallization. The increase in the amplitude of the fluctuations is believed to be a result of the segregation of noncrystallizable components (crosslinked points) from crystallizable components (chains between the crosslinked points) and subsequent crystallization in the regions rich in crystallizable chains. This crystallization behavior has the characteristics of spinodal crystallization, as discussed previously, which is for the first time elucidated for the oriented crystallization of crosslinked chains in this work.

Some of this work was conducted in the framework of the Japan–Poland Government Agreement on Scientific Cooperation through funds directed to the Institute of Fundamental Technological Research of the Polish Academy of Sciences when one of the authors (A.W.) was employed there. The authors gratefully acknowledge Andrzej Ziabicki, the late Hiromichi Kawai, and the late Marian Kryszewski for their enlightening comments and encouragement of this work.

References

1. Koch, M. J. H.; Bordas, J.; Schola, E.; Broecker, H. C. Polym Bull 1979, 1, 709.
2. Schultz, J. M. In Polymer Research at Synchrotron Radiation Sources; Russel, T. P.; Goland, A. N., Eds.; 1984.
3. Saijo, K.; Wasiak, A.; Suehiro, S.; Kawai, H.; Hashimoto, T. Preprints of the First SPSJ International Polymer Conference, Kyoto, Japan, 1974; Soc. Polym. Sci. Jpn. p 275,
4. Saijo, K.; Hashimoto, T.; Wasiak, A. Time-Resolved SAXS and WAXS Studies on Oriented Crystallization in Crosslinked cis-1,4-polybutadiene, NATO Advanced Studies Institute: Caminha, Portugal, 1999.
5. Mandelkern, L. Crystallization of Polymers; McGraw-Hill: New York, 1964.
6. Wunderlich, B. Macromolecular Physics; Academic: New York, 1976; Vol. 2.
7. Mandelkern, L. In Comprehensive Polymer Science; Allen, G.; Bevington, J. C., Eds.; Pergamon: Oxford, 1989; Vol. 2.
8. Crystalline & Noncrystalline Solids; Hannay, N. B., Ed.; Plenum: New York, 1976; Vol. 3.
9. Kratky, O.; Glatter, O. Small Angle X-Ray Scattering; Academic: New York, 1982.

10. Takserman-Krozer, R. J Polym Sci 1967, 16, 2855.
11. Ziabicki, A.; Jarecki, L. J Chem Phys 1994, 101, 2267.
12. Stein, R. S.; Judge, J. T. J Appl Phys 1961, 32, 2357.
13. Kawai, T.; Iguchi, M.; Tonami, H. Kolloid Z 1967, 221, 28.
14. Keller, A.; Machin, M. J. J Macromol Sci Phys 1967, 1, 41.
15. Katayama, K.; Amano, T.; Nakamura, K. Kolloid Z 1968, 226, 125.
16. Hill, M. J.; Keller, A. J Macromol Sci Phys 1969, 3, 153.
17. Kobayashi, K.; Nagasawa, T. J Macromol Sci Phys 1970, 4, 351.
18. Hill, M. J.; Keller, A. J Macromol Sci Phys 1971, 5, 591.
19. Sietz, W.; Goritz, D.; Muller, F. M. Colloid Polym Sci 1974, 252, 854.
20. Gent, A. N. Trans Faraday Soc 1954, 50, 521.
21. Mandelkern, L. Crystallization of Polymers; Wiley: New York, 1964.
22. Gent, A. N. J Polym Sci Part A-2: Polym Phys 1966, 4, 447.
23. Kim, H. G.; Mandelkern, L. J Polym Sci Part A-2: Polym Phys 1968, 6, 181.
24. Kitamaru, R.; Chu, H.-D.; Tsuji, W. Int Symp Macromol 1966, 8, 98.
25. Akana, Y.; Stein, R. S. J Polym Sci Polym Phys Ed 1975, 13, 2195.
26. Scholtens, B. J. R.; Riande, E.; Mark, J. E. J Polym Sci Polym Phys Ed 1984, 22, 1223.
27. De Candia, F.; Romano, G.; Russo, R.; Vittoria, V. J Polym Sci Polym Phys Ed 1982, 20, 1525.
28. De Candia, F.; Romano, G.; Russo, R.; Vittoria, V. J Polym Sci Polym Phys Ed 1982, 23, 2109.
29. Alfonso, G. C.; Verdona, M. P.; Wasiak, A. Polymer (London) 1978, 19, 711.
30. Chirico, A. D.; Lanzani, P. C.; Ragga, E.; Bruzzone, M. Macromol Chem 1974, 175, 2029.
31. Natta, G.; Corradini, P. Angew Chem 1956, 68, 615.
32. Suehiro, S.; Saijo, K.; Ohta, Y.; Hashimoto, T.; Kawai, H. Anal Chim Acta 1986, 189, 41.
33. Saijo, K.; Hashimoto, T. Mater Res Soc Symp Proc 1987, 79, 267.
34. Hashimoto, T.; Saijo, K.; Kosc, M.; Kawai, H.; Wasiak, A.; Ziabicki, A. Macromolecules 1985, 18, 472.
35. Strobl, G. R.; Schneider, M. J Polym Sci Polym Phys Ed 1980, 18, 1343.
36. Guinier, A.; Fournet, G. Small-Angle Scattering of X-Rays; Wiley: New York, 1955.
37. Gaylord, R. J. J Polym Sci Polym Phys Ed 1976, 14, 1827.
38. Flory, P. J. J Chem Phys 1947, 15, 397.
39. Cahn, J. W. Trans Met Soc AIME 1968, 242, 166.
40. Hashimoto, T. Phase Transitions 1988, 12, 47.
41. Hashimoto, T. In Material Science and Technology; Cahn, W. R.; Haasen, P.; Kramer, E. J., Eds.; Structure and Properties of Polymers 12; VCH: Weinheim, 1993; p 251.
42. Petermann, J.; Gohil, R. M.; Schultz, J. M.; Hendricks, R. W.; Lin, J. S. J Polym Sci Polym Phys Ed 1982, 20, 523.
43. Petermann, J. Makromol Chem 1981, 182, 613.
44. Imai, M.; Mori, K.; Mizukami, T.; Kaji, K.; Kanaya, T. Polymer 1992, 33, 4457.
45. Kaji, K.; Nishida, K.; Kanaya, T.; Matsuba, G.; Konishi, T.; Imai, M. Adv Polym Sci 2005, 191, 187.
46. Olmsted, P. D.; Poon, W. C. K.; McLeish, T. C. B.; Terill, N. J.; Ryan, A. J. Phys Rev Lett 1998, 81, 373.
47. Ryan, A. J.; Terill, N. J.; Fairclough, J. P. A. Study of Nucleation Phenomenon in Homopolymer Melts; NATO Advanced Studies Institute: Caminha, Portugal, 1999.
48. Inaba, N.; Sato, K.; Suzuki, S.; Hashimoto, T. Macromolecules 1986, 19, 1690.
49. Brazovskii, S. A. Sov Phys JETP 1975, 41, 85.
50. Krigbaum, W. R.; Ciferri, A. Mol Cryst Liq Cryst 1981, 61, 273.
51. Goeritz, D.; Zietz, R.; Kreitmeier, S.; Wittkop, M.; Wagner, T. Colloid Polym Sci 1995, 273, 1008.
52. Treloar, L. R. G. The Physics of Rubber Elasticity; Oxford University Press: London, 1958.